REPUBLIC OF TURKEY

YILDIZ TECHNICAL UNIVERSITY

GRADUATE SCHOOL OF NATURAL AND APPLIED SCIENCES

EMPLOYING OF A HYDROPHOBIC MEMBRANE FOR RAPID REMOVAL OF GASES IN THE PLANAR MICROFLUIDIC ELECTROLYZER

Nurdan MESE

MASTER'S THESIS

Department of Chemical Engineering

Chemical Engineering Program

Advisor

Prof. Dr. Hasan SADIKOGLU

Co-Advisor

Assist. Prof. Dr. Muhammed Enes ORUC

January, 2021

REPUBLIC OF TURKEY

YILDIZ TECHNICAL UNIVERSITY

GRADUATE SCHOOL OF NATURAL AND APPLIED SCIENCES

EMPLOYING OF A HYDROPHOBIC MEMBRANE FOR RAPID REMOVAL OF GASES IN THE PLANAR MICROFLUIDIC ELECTROLYZER

A thesis submitted by Nurdan MESE in partial fulfillment of the requirements for the degree of **MASTER** is approved by the committee on 12.01.2021 in the Department of Chemical Engineering, Chemical Engineering Program.

Prof. Dr. Hasan SADIKOGLU	Assist. Prof. Dr. Muhammed Enes ORUC
Yıldız Technical University	Gebze Technical University
Advisor	Co-Advisor

Approved By the Examining Committee

Prof. Dr. Hasan SADIKOGLU, Advisor
Yıldız Technical University ______________________________

Prof. Dr. Fatma Jale GULEN, Member
Yldız Technical University ______________________________

Assoc. Prof. Dr. Mahmut SEKER, Member
Zonguldak Bulent Ecevit University ______________________________

I hereby declare that I have obtained the required legal permissions during data collection and exploitation procedures, that I have made the in-text citations and cited the references properly, that I haven't falsified and/or fabricated research data and results of the study and that I have abided by the principles of the scientific research and ethics during my Thesis Study under the title of Employing of a Hydrophobic Membrane for Rapid Removal of Gases in the Planar Microfluidic Electrolyzer supervised by my supervisors, Prof. Dr. Hasan SADIKOGLU and Assist. Prof. Dr. Muhammed Enes ORUC. In the case of the discovery of a false statement, I am to acknowledge any legal consequence.

Nurdan MESE

Signature

Dedicated to my family

ACKNOWLEDGEMENTS

I would like to express my thanks to people without whom I could not complete this study. I want to start my thesis advisors Prof. Dr Hasan SADIKOGLU and Assist. Prof. Dr. Muhammed Enes ORUC, for their endless guide, support and patience. It was a great honor and pleasure to work with them and benefit from their scientific experiences, creative way of thinking, excitement and teaching methods.

I would like to express my infinite thanks to Sevde OMEROGLU, Kubra ERDOGAR and other members of Oruc Lab in Gebze Technical University for their support and advice.

I am also grateful to Assist. Prof. Dr. Hakan YILMAZER from Yildiz Technical University, Department of Materials Science and Engineering, for his advice and support regarding studies of metal surface treatments in his lab.

I especially would like to thank my family, my father Enver MESE, my mother Halime MESE, my sisters Bahar MESE and Pınar KESKIN, and Erdem KESKIN for their support whenever I need and whatever the case. They support my studies and encourage me to proceed for all my life. Also, I was able to overcome challenges with the existence of Masal KESKIN, who gives me the strength to struggle.

Finally, my special feeling of gratitude to Recep COCUK. Without his support, I would not have completed this study.

Nurdan MESE

TABLE OF CONTENTS

LIST OF SYMBOLS

CO_2	Carbon Dioxide
CO	Carbon Monoxide
A	Electric Current
V_{cell}	Electrolysis Cell Potential Required for Electrolysis
ΔH	Enthalpy Change
ΔS	Entropy Change
F	Faraday's Constant
ΔG	Gibbs Energy Change
ΔG°	Gibbs Free Energy
H_2	Hydrogen Gas
OH^-	Hydroxide Ion
Ir	Iridium
Ni	Nickel
η	Overall Electrolysis Efficiency
Pt	Platinum
KOH	Potassium Hydroxide
K^+	Potassium Ion
V_{rev}	Reversible Cell Voltage
NaOH	Sodium Hydroxide
Na^+	Sodium Ion
ΔH°	Standard Enthalpy Value
SO_3H	Sulfonic Acid
Q	Thermal Energy
V_{th}	Thermoneutral Cell Voltage
C	Total Quantity of Charge Transferred
z	Transferred Electrons Number/Hydrogen Molecule

LIST OF ABBREVIATIONS

CAD	Computer-aided Design
CE	Counter Electrode
DC	Direct Current
DSA	Double-sided Adhesive
G	Ground Connection
PDMS	Polydimethylsiloxane
PEM	Polymer Electrolyte Membrane
PMMA	Polymethylmethacrylate
PP	Polypropylene
PTFE	Polytetrafluoroethylene
PV	Photovoltaic
RE	Reference Electrode
S	Sense Electrode
SO	Solid Oxide
3D	Three-dimensional
2D	Two-dimensional
VOCs	Volatile Organic Compounds
WE	Working Electrode

LIST OF FIGURES

LIST OF TABLES

ABSTRACT

Employing of a Hydrophobic Membrane for Rapid Removal of Gases in the Planar Microfluidic Electrolyzer

Nurdan MESE

Department of Chemical Engineering

Master of Science Thesis

Advisor: Prof. Dr. Hasan SADIKOGLU

Co-advisor: Assist. Prof. Dr. Muhammed Enes ORUC

Energy is a basic need for the growing world population. Hydrogen as an energy carrier is a solution to several challenges, such as the detrimental effects of fossil fuels and the depressing of fluid hydrocarbons reserves. Although hydrogen is clean and safe, various hydrogen production methods (e.g. steam methane reforming and partial oxidation) use non-renewable energy sources. As a viable alternative to these, water electrolysis is commonly employed. Planar micro electrolyzers for hydrogen production have advantageous since their affordable installation, portability, and easier integration to other systems. The main challenge of electrolysis in microfluidic systems is the gas management. The gas-phase causes an additional friction to flow leading to microchannels clogging and a reduction in the contact area between the electrode and the electrolyte. For this purpose, we designed and fabricated a planar microfluidic alkaline water electrolyzer, proposing a hydrophobic membrane on top of the electrodes to provide a rapid gas removal from the electrodes and improve hydrogen production efficiency. We examined whether the contribution of the membrane, which allows the diffusion of generated gases to the other side of the membrane, performing the same operating conditions in both membraneless and membrane-embedded electrolyzers. We investigated the effect of flow rate and temperature at various potentials and currents on hydrogen production. The highest overall electrolysis efficiency was achieved in the membrane-embedded electrolyzer at 65 ˚C and 5 ml/min as the optimum operating condition. Therefore, our results show that embedding the hydrophobic membrane to the planar electrolyzer provides a significant achievement regarding hydrogen production efficiency for our design.

Keywods: Energy, hydrogen production, two-phase flow, planar microfluidic electrolyzers, hydrophobic membrane

Düzlemsel Mikro Elektrolizörlerde Oluşan Gazların Hızlı Giderimi için Hidrofobik Membran Kullanımı

Nurdan MEŞE

Kimya Mühendisliği Bölümü

Yüksek Lisans Tezi

Danışman: Prof. Dr. Hasan SADIKOĞLU

Eş-Danışman: Dr. Öğr. Üyesi Muhammed Enes ORUÇ

Enerji, artan dünya nüfusu için temel bir ihtiyaçtır. Bir enerji taşıyıcı olarak hidrojen, fosil yakıtların olumsuz etkileri ve akışkan hidrokarbon kaynak rezervlerinin azalması gibi pek çok soruna çözüm olarak kullanılabilir. Hidrojen temiz ve güvenli olmasına karşın, metan buhar reformasyonu ve kısmi oksidasyon gibi pek çok hidrojen üretim yöntemi yenilenemez enerji kaynaklarını kullanır. Tüm bunlara alternatif olarak suyun elektrolizi yaygın olarak kullanılmaktadır. Hidrojen üretimi için düzlemsel mikro elektrolizörlerin kullanımı uygun fiyatlı kurulum, taşınabilirlik ve diğer sistemlere daha kolay entegrasyon gibi sebeplerden dolayı oldukça avantajlıdır. Mikroakışkan sistemlerde gerçekleştirilen elektroliz için en temel zorluk gazların kanallardan giderimidir. Gaz fazı akışta ekstra sürtünmeye yol açarak mikrokanalların tıkanmasına ve elektrot ile elektrolit arasındaki temas alanının azalmasına neden olmaktadır. Bu amaçla, elektrotlardan hızlı gaz uzaklaştırılması ve hidrojen üretim veriminin arttırılması için elektrot üzerine hidrofobik bir membran yerleştirilmesini önererek düzlemsel mikroakışkan alkali elektrolizörlerin tasarımını ve fabrikasyonunu gerçekleştirdik. Membransız ve membranlı sistemlerde eşit operasyon koşullarını sağlayarak, önerdiğimiz membranlı sistemde gazların difüzyonuna katkısını gözlemledik. Farklı potansiyel ve akım değerlerinde akış hızı ve sıcaklık parametrelerinin hidrojen üretimine etkisini inceledik. Hidrojen üretiminin en yüksek elde edildiği optimum koşulu olarak 65 ˚C sıcaklık ve 5 ml/dk akış hızı bulundu. Sonuç olarak, elektrolizör tasarımımıza seçtiğimiz hidrofobik membranın entegre edilmesinin hidrojen üretiminde önemli gelişmeler sağladığını gözlemlendi.

Anahtar Kelimeler: Enerji, hidrojen üretimi, iki-fazlı akışlar, düzlemsel mikroakışkanlı elektrolizörler, hidrofobik membranlar

1
INTRODUCTION

1.1 Literature Review

1.1.1 Energy Demand and Hydrogen

Humanity inevitably needs energy due to population growth and ever-increasing living standards in the world. Energy consumption has been increasing as a result of urbanization and industrialization. It is acceptable that there is a correlation between available energy and the national economy. Therefore, different energy utilization methods have been investigated all over the world to benefit from alternative energy sources. Hydrogen would be an efficient alternative energy carrier to fulfil the energy needs of the world because it is clean, safe, and reliable, which can be used in different sectors such as transportation, cooling, and heating, housing applications, petrochemical processes, fertilizers, and fuel cells [1-3]. Hydrogen is an odourless and non-toxic element that is the lightest of the periodic table. It can be stored and transported, and while comparing to traditional fuels, it does not have carbon emission, producing only water while burning [4-6]. Hydrogen is an abundant supply; however, it is not found in a free state in nature, and different processes are necessary to obtain hydrogen elements. Although it occupies an important position as an energy carrier because of its cleanliness, today most of the hydrogen (>96 %) is produced from non-renewable resources that are not sustainable and releasing greenhouse gases to the atmosphere [3, 7]. Some of these production methods are steam methane reforming, partial oxidation, and coal gasification [4]. These methods are preferable due to their cheapness; however, hydrogen production from renewable resources should be increased to reduce carbon emission and dependence on fossil fuels, which are significant concerns growing day by day all over the world. Methods using renewable resources are hydrogen production in the form of biomass processes and electrolysis method that use water only [2]. Biomass processes can be categorized into thermochemical and biological processes. Pyrolysis, gasification, combustion, and liquefaction can be included in the thermochemical subgroup. Fundamentally, hydrogen-rich gases are transformed from biomass with approximately 35-50 % efficiency in these methods. Regarding advantages, the feedstock is abundant and cheap as well as no additional carbon dioxide (CO_2) is releasing into the atmosphere (CO_2-neutral) during thermochemical processes. However, these methods suffer from impurities in the raw material, tar formation, and variable hydrogen gas (H_2) content since feedstock depends on the season. Biological processes mainly encompass direct and indirect biophotolysis, photo, and dark fermentations, and sequential dark and photo-fermentation. It is possible to operate these processes at standard temperature and pressure. Therefore, one advantage of biological processes is less energy-consuming. Although depending on the production methods, significant drawbacks of biological processes are indicated below [8, 9].

- Sunlight is necessary, which leads to seasonal changes for H_2 content.
- Low H_2 production efficiency are achieved.
- Reactor volume should be maximized.

On the other hand, a convenient way to reduce dependency on fossil fuels and detrimental effects on the environment is using water for hydrogen production. In this approach, water directly decomposes to hydrogen and oxygen. For this method, the necessary electricity should be generated from renewable resources such as solar photovoltaic (PV) cells [10], wind turbines, solar and geothermal energy, which are environmentally friendly and sustainable; hence, there are almost no greenhouse gases and air pollutants such as volatile organic compounds (VOCs), carbon monoxide (CO), SO_x, NO_x. Oruc et al. [11] integrated an alkaline planar water electrolyzer with a PV thermal technology module to improve electrical efficiency. Gibson et al. [12] performed the optimization process of the PV-electrolysis system by adapting the operation voltage of the polymer electrolyte membrane (PEM) electrolyzer with maximum power output and voltage of PV's to increase the hydrogen production efficiency. Although there are several papers in the literature, the development of the current systems and new approaches are required because the performance of renewable sources varies according to location and time. In addition, there are challenges regarding the storage and transportation of the produced energy. The future of the hydrogen economy mainly depends on low-cost assembly techniques and the existence of renewable sources [13].

1.1.2 Challenges in Low-Temperature Water Electrolysis

Although electrolytic processes for pure hydrogen production is one of the most viable alternatives to fossil energy sources, these processes may bring several challenges, overpotential or losses, leading to an efficiency decrease and an increase in power consumption. These challenges need to be faced with producing highly efficient and cheaper electrolyzers in the industrial stage. Overpotentials can be categorized into two types, named as the activation and the ohmic overpotentials. During an electrochemical reaction, additional voltage is necessary to overcome the activation energies, which refer to as activation overpotential. In addition, resistances related to the electrode, electrolyte, and membrane are in the category of ohmic overpotentials. One significant reason causing the overpotentials is the gas generation on the electrode surface that increases the ohmic losses. Gas formation is inevitable; therefore, over the years, researchers have been focusing on gas management studies. Although there are several studies investigating gas bubble or two-phase flow behaviours, gas management in microfluidics has caught little attention in the literature. Pierre Jonville [14] firstly offered gas removal in 1978. They obtained a patent which was named electrolyzer with released gas. The purpose of this invention was to present a gas bubble release in an electrolyzer with an electrode covered by a porous layer that was permeable to gas to prevent the electrode polarization and the loss of electrochemical efficiency of the electrolysis. Currently, traditional gas prevention methods for microfluidic devices are generally ineffective because of various reasons. The flushing of microchannels before the operation is the most popular by employing aqueous solutions with low polarities, such as ethanol, methanol, or isopropanol, which is an extra step. Besides, although microchannels are flushed, gas bubbles may still stick to the corners or various surfaces even at hydrophilic microchannel surfaces treated with oxygen plasma to prevent gas bubble adhesion. Another method, which is defined as bubble-trap integration to microdevices, has limitations in terms of low trapping volume because of their small size. When bubble-trap gets full of gas bubbles during the operation, the microchannel begins suffering from clogging. These passive methods can be addressed with the methods removing gases simultaneously; for instance, using a gas-permeable membrane. Four significant criteria should be satisfied to provide gas management with a gas-permeable membrane [15-17].

- A more considerable bubble length than channel height is required.
- Gases require sufficient time to stay on the membrane for effective gas removal.
- The gas flow rate should be maintained below a critical value to prevent a stagnant liquid film between the gas and the membrane. (This film blocks the mass transfer.)
- The pressure drop across the membrane should be below the Laplace pressure to prevent leakage of the liquid phase.

Regarding gas management studies, Jiang et al. [7] reported a planar alkaline microfluidic electrolyzer design for gas bubble separation by flowing force of the electrolyte on the bubble and analyzing reactor flow pattern while producing hydrogen. They focused on the rapid extraction of bubbles resting on the electrode surface, which is a combination of buoyancy, superficial tension, flow pressure, inertia, and electrostatic forces. Electrode configuration and microfluidic chamber design were essential criteria to obtain proper flow for gas detachment. Additionally, they calculated the average bubble radius and detachment rate from the variable voltage potentials. Nagai et al. [18] determined the hydrogen production efficiency according to the gas bubbles between electrodes and proposed the optimum space of them by considering other parameters, e.g. current density, temperature, pressure, height, width, inclination, wettability of electrodes during water electrolysis. Hydrogen and oxygen bubbles between electrodes lead to an increase in void fraction, which eventually leads to higher electric resistance when the current density was up to 0.6 A/cm^2. On the other hand, if the current density was higher than this value, the voltage increased. Therefore, it was essential to determine the optimum space between electrodes while designing an electrolyzer to perform gas management properly. Another study belonging to Nagai et al. [19]

demonstrated the relationship between bubble rising velocity and current density. They calculated optimum conditions of bubble rising velocity, current density, and bubble diameter. Winther-Johnson et al. [20] designed a novel electrode to separate bubbles easily from hydrophobic membrane (Goretex) electrodes to improve the efficiency of the electrolysis process. Vilasmongkolchai et al. [21] described an electrolyzer having a pulse-activated system to increase hydrogen production efficiency with no extra bubble. They estimated the mathematical model of rest period with parameters of the bubble's radius, inside and outside bubble density difference, gravitational acceleration, and electrolyte's dynamic viscosity.

Derami et al. [22] proposed an efficient method to remove gas bubbles from microchannels (various 100 to 300 μm) by embedding polytetrafluoroethylene (PTFE) membranes containing various pore sizes from 0.45 to 3 μm. Moreover, they computed a three-dimensional (3D) fluid model to compare gas removal efficiency with their experimental results. The theoretical and experimental results were similar, and they confirmed gas permeability of the membrane increased with the growing pore size. Tiwari et al. [23] devised a bubble-free electrolyzer by using electrodes consisting of the Gortex gas diffusion layer and catalyst coating. Bubbles at each electrode were removed with the help of the gas-philic layer, and the highest known intrinsic efficiency was obtained. Cho et al. [15] provided a microfluidic device with a top disposable layer, which supplies an active bubble removal with the help of a polydimethylsiloxane (PDMS) membrane which is positioned at the bottom of the microchannel. An integrated vacuum trench applied low pressure toward the bottom to push gases through membrane pores. They concluded that the degassing rate is faster comparing to passive gas removal methods. Oruc et al. [24] designed a micro electrolyzer that can be integrated with a PV cell to generate hydrogen efficiently by removing clogging gases in the microchannel. They determined optimum parameters that are channel dimensions, electrolyte temperature and flow rate, and pulsed, or continuous operation mode.

1.2 The Objective of the Thesis

During electrolysis, the generated gases within the microchannels induce a considerable reduction in the interaction area between the electrode and the electrolyte. This undesirable phenomenon decreases the efficiency of hydrogen production. Although higher flow rates are applied to the channels, it is difficult to get rid of the gas bubbles. Therefore, this thesis aims to use a hydrophobic porous membrane in our microfluidic planar electrolyzer design to produce hydrogen more efficiently. Our first objective is to demonstrate that the hydrophobic membrane transfers the generated gases on the electrodes to the other side of the membrane and eliminates the bubble blockage problem in the microchannels of the electrolyzer. Our second goal is to investigate the parameters of flow rate, temperature, and applied voltage that affect the hydrogen production rate.

1.3 Hypothesis

If a microfluidic planar water electrolyzer consisting of an appropriate hydrophobic porous membrane design, it will provide the removal of the accumulated gases on the electrode surface, which means that blockage of the microfluidic chamber with bubbles can be addressed and will yield a higher amount of hydrogen production. Thus, we hypothesize that employing a PTFE hydrophobic porous membrane will only allow gas diffusion and resist the electrolyte passing through it. This design will provide gas management within the electrolyzer.

2
THE HYDROGEN PRODUCTION TECHNOLOGIES FROM WATER ELECTROLYSIS

2.1 Introduction

Water is an important source to produce hydrogen. Pure hydrogen is obtained eligibly from the water electrolysis method comparing to the source of fossil fuels. Besides, no carbon emission indicates the reliability of the technique regarding environmental issues. The efficiency of the electrolyzers varies between 70% and 90%, depending on the electrolysis method, components, or operating conditions. Thermolysis and solar thermochemical cycles use water for hydrogen production [25]. The former directly uses a high temperature up to 2225 °C to decompose water into hydrogen gas (H_2) and oxygen gas (O_2). Although it can tolerate fluctuations of operation temperature, an effective separation technique of H_2 and O_2 should be developed because hazardous gases may form if it is directly cooled. The separation problem of H_2 and O_2 can be mitigated in solar thermochemical cycles; however, one drawback is that it requires several reaction stages, including one endothermic, and then exothermic steps. This case leads to an increase in inefficiencies [26]. On the other hand, the future hydrogen economy can be managed with the development of current water electrolysis technologies [23].

Commercially, water electrolysis technologies may have limitations such as the consumption of higher energy, the necessity of noble metals usage like platinum, pure dynamic response to load changes, and assembly difficulties [27]. Studies have been conducted related to water electrolysis technologies to combat economic restrictions and develop more efficient systems [3]. The European Commission has set a target for a new clean hydrogen strategy to help to decarbonize more cheaply by 2050. In Figure 2.1, their strategy has been illustrated. The European Commission has operated studies to gather evidence regarding clean hydrogen production techniques. Until 2024, assembly of electrolyzers utilizing renewable resources sources, and hydrogen production from these electrolyzers (at least 1 million tonnes hydrogen) have been encouraged. Then, the central part of the European energy system will be provided by renewable hydrogen electrolyzers and hydrogen production from them up to 10 million tonnes between the years 2025-2030. After 2030, hydrogen from renewable resources sources will spread out across Europe.

Figure 2.1 The path towards a European hydrogen eco-system step by step [28].

2.2 The Current Water Electrolysis Technologies

Generally, in the water electrolysis process, a direct current (DC) is applied to decompose water into its elements (hydrogen and oxygen) as chemical energy. Two electrodes, cathode and anode with a certain distance, are immersed in an electrolyte. The electrodes are selected according to different criteria such as corrosion resistance, electric conductivity, and structural integrity. Flowing ions complete the charge exchange with the help of electrolytes. Reduction half-reaction takes place on the cathode, and oxidation half-reaction occurs on the anode to produce hydrogen and oxygen gases, respectively [6].

All electrolysis methods have the same overall reaction indicated below [3];

$$H_2O_{(l)} \longrightarrow H_{2(g)} + 1/2\ O_{2(g)} \qquad (2.1)$$

Theoretical voltage values of the equilibrium are 1.23 V and 1.18 V at 25 °C and 80 °C, respectively. However, commercial electrolyzers operate at higher voltages because of the overpotentials [23].

The main electrolysis techniques are PEM electrolysis, solid oxide (SO) electrolysis, and alkaline water electrolysis.

Polymer Electrolyte Membrane (PEM) Electrolysis

One of the most common types of electrolysis is known as PEM electrolysis, which uses a proton exchange membrane providing ionic permeability to produce hydrogen [29]. This membrane allows the transition of proton ions from the anode to the cathode to recombine with the electron. It has an acidic feature because of the sulfonic acid (SO_3H) functional groups that increase proton conductivity. The most outstanding feature of this type of electrolyzers is hydrogen purity which is reached to 99.999% in some operations due to low gas crossover of the membrane. Furthermore, high current densities, wide load range, good dynamic response, and high operating pressures up to 85 bar are potential benefits of the technique [6]. However, these types of electrolyzers contain certain limitations such as high assembly cost, low durability because of the short life of electrolyzer, the restricted capacity of hydrogen production, and the necessity of noble metals usage like iridium (Ir), and platinum (Pt). Therefore, they are used in small-scale applications that have a low capacity for hydrogen production.

Solide Oxide (SO) Electrolysis

SO electrolyzers use steam as a reactant due to high operating temperatures varied between 600-1000 ˚C. High operation temperature provides lower electricity consumption. The reason behind the deep interest in this technique is the production of ultra-high purity of hydrogen and greater efficiencies. At the cathode, steam is reduced to produce hydrogen and oxide ions, and a solid ceramic electrolyte is permeable the oxide anions to the anode [3]. The issues that need to be overcome are the fast degradation rate of a cell, the assembly costs, and the lack of stability [6].

Alkaline Water Electrolysis

In this method, oxidation and reduction half-reactions occur at the separated electrode surfaces by applying a DC. An external circuit connects these electrodes to complete the electrolysis reaction. Ionic charges transport via electrolyte whose concentration is generally varied between 20%-30% potassium hydroxide (KOH) or sodium hydroxide (NaOH), maximizing ionic conductivity. Initially, water reduction takes place on the cathode surface to produce hydrogen gas and charge carrier hydroxide ions (OH^-), following which the electric field transfers these anions to the anode to produce oxygen gas and electrons. Half-reactions for the cathode and the anode are as follows, respectively [6].

$$2H_2O_{(l)} + 2e^- \longrightarrow H_{2(g)} + 2OH^-_{(aq)} \tag{2.2}$$

$$2OH^-_{(aq)} \longrightarrow \frac{1}{2} O_{2(g)} + 2e^- \tag{2.3}$$

This electrolysis method is the most commercially developed and compatible with renewable energy sources like hydropower, photovoltaics, and wind energy [30]. Both small and large-scale productions may be obtained through this method. System efficiency is moderate, and the current density is relatively lower than the other two methods [29]. These types of electrolyzers have positive and negative features. Although high durability [4], usage of any type of metals as an electrode, reduced capital cost, and longevity of devices [6] can be accepted as advantages, limited current densities, low operation conditions regarding temperature and pressure, low partial load range [31], corrosion capacity of highly concentrated electrolyte [6] can be listed as drawbacks. Operation pressure varies from atmospheric pressure up to 10-30 bars [32]. Operation temperature is generally below 100 ˚C resulting in a relatively low electrolyte conductivity and slow electrochemical reaction kinetics. However, there are advanced alkaline water electrolyzers having higher operating temperatures up to 150 ˚C [6].

2.3 Thermodynamics and Energy Efficiency of Electrolysis

In alkaline water electrolyzers, water decomposition begins when DC is applied to electrodes separated by an alkaline electrolyte. For the water decomposition reaction, several assumptions are necessary. Some of them are indicated below.

- Different phases are accepted as separate.
- Hydrogen and oxygen gases are ideal.
- The liquid phase is incompressible.

To compose a thermodynamic model, enthalpy change (ΔH), entropy change (ΔS), and Gibbs free energy change (ΔG) of water splitting reaction should be calculated.

Change in Gibbs free energy representing the minimum energy amount supplied by electricity is obtained by using

$$\Delta G = \Delta H - T\Delta S = \Delta H - Q \qquad (2.4)$$

where Q is the thermal energy equivalent to TΔS, where T is the electrolysis temperature, and ΔS is the entropy change [33, 34]. The lowest voltage required for water splitting reaction is known as the reversible cell voltage (V_{rev}) and can be expressed as below

$$V_{rev} = \frac{\Delta G}{zF} \qquad (2.5)$$

where z is the transferred electrons number/hydrogen molecule (2 for water splitting reaction via electrolysis), and F is the Faraday's constant which is 96485 C/mol [11]. When the only source providing thermal energy TΔS is the electricity with no thermal effects, there is a correlation between total energy demand and thermoneutral cell voltage (V_{th}) represented below

$$V_{th} = \frac{\Delta H}{zF} \qquad (2.6)$$

The splitting of water is an endothermic reaction; hence, the required total energy amount is equal to the enthalpy change. The standard enthalpy value (ΔH°) for water splitting is 286 kJ/mol. This reaction is also non-spontaneous at standard conditions (25 ˚C, 1 bar). At these conditions, Gibbs free energy (ΔG°) is 237 kJ/mol, and equal to the necessary amount of work for water decomposition [11].

At standard conditions, electrolysis reversible and thermoneutral cell voltages are calculated as Vrev = 1.229 V and Vth = 1.482 V, respectively. The correlation between these voltages and temperature theoretically can be seen in Figure 2.2 [35]. Temperature and pressure changes affect enthalpy voltage slightly since enthalpy change remains almost constant because of thermal energy changes balancing with the Gibbs' free energy change at different temperatures [34]. For operation temperatures that we studied, theoretical electrolysis voltage values are 1.229, 1.217, and 1.196 at the temperatures of 25 ˚C, 40 ˚C, and 65 ˚C, respectively.

The following equation can be used to calculate the overall efficiency of water electrolysis at standard conditions [11].

$$\eta = \frac{V_{rev}^{\circ}}{V_{cell}} = \frac{1.229}{V_{cell}} \tag{2.7}$$

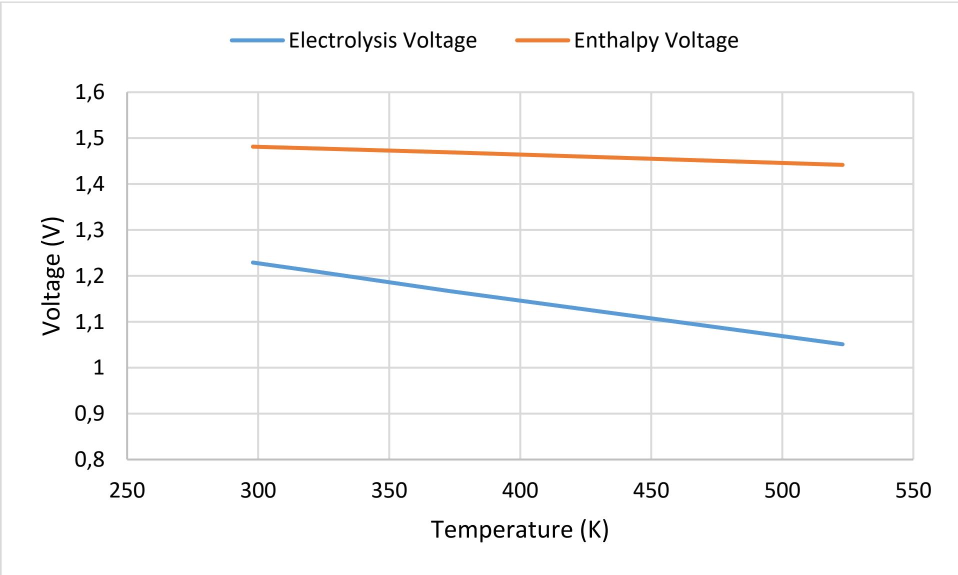

Figure 2.2 Electrolysis and enthalpy voltages versus temperature at 1 atm pressure.

3
MEMBRANE INTEGRATION INTO MICROFLUIDIC DEVICES

3.1 Two-Phase Flow

Two-phase flow has become more critical day by day as many engineering applications; for instance, synthesis, separation, and purification benefit from its advantages [36]. Single-phase transfer systems have been replaced with phase change transfer systems with the advent of technological developments, resulting in transport and thermal mitigations for different industries (heating, nuclear power, and ventilation). However, all industries using multiphase systems may encounter various drawbacks [37]. One of the main reasons for these challenges stems from the different physical properties of each phase. For example, while the gas-phase is compressible, the liquid phase is assumed as incompressible. Moreover, the density of the liquid phase is higher than the density of the gas-phase [38].

The instabilities are another problem in two-phase flow applications. Different modes of two-phase instabilities (static or dynamic) adversely affect the system performance, and they make the design of multiphase flow devices difficult. Therefore, a designer should take into consideration two-phase flow challenges in all details. Extensive studies regarding two-phase flow have been conducted for more than 100 years, yielding theoretical and commercial achievements. Despite improvements, two-phase flow systems still bring several problems in their applications, especially for micro-sized devices. For macro-dimensional devices, the management of gas-liquid flow is easier. When dimensions are reduced; however, two-phase flow leads to different challenges. Some problems regarding two-phase flow in micro-sized devices are concluded below

- Volume change occurs while transferring gas and liquid phases between each other.

- Gas-phase is easily affected by contaminations of different components, leading to a change in the stability of flow [38].
- Pressure-drop rises during gas-phase growth [39].

Many researchers with the aim of increasing usage of microfluidic systems in various applications, such as compact heat exchangers or supercomputers have been devised novel variations of them to solve the aforementioned two-phase flow problems. For instance, a pressure drop is a primary parameter, which is densely studied, characterizing power consumption alongside the microfluidic channels [40]. Another essential parameter is a gas void fraction in two-phase flow while designing a device or system since various determinations (e.g. pressure drop, heat transfer coefficient as well as flow characterization) can be expressed with the use of this parameter [41]. Calculation methods of gas void fraction vary based on different applications. While flow's visual images are utilized in optical methods, acoustic impedance change is determined in ultrasonic transmission techniques. γ-ray or X-ray attenuation and wire mesh tomography are other techniques that are generally employed. Studies regarding the calculation of this parameter have been still carried out as these methods are mostly intrusive, complicated, expensive, and not applicable [42]. Barreto et al. [43] performed a study to calculate pressure drop and void fraction of gas in microchannels, transferring gas-liquid two-phase flow in several flow patterns. They verified experimentally whether available methods were applicable.

Moreover, in microchannels, the mixing of gas and liquid phases can be categorized into active mixing and passive mixing. Continuous flow is generally performed at laminar conditions, which tends to result in passive mixing, limiting heat and mass transfer between separate phases. Gas bubble mobility is also affected by the flow pattern. According to the relationship between bubble size and surface mobility, if a spherical bubble diameter is lower than 2 mm, the bubble performs as a solid particle and cannot move through flow. For spherical diameter values higher than 5 mm; however, bubbles can become mobile freely. While rigid bubbles have regular shapes, mobile bubbles can change their shape easily; thus, it can be removed by turbulent flow [44]. Bao et al. [45] discussed the effects of turbulence flow on single bubble transfer to observe mass transfer between gas and liquid phases. Additionally, they used different models as Higbie, Frossling, and Lamont and Scott to compare mass-transfer coefficients. They concluded mass transfers were affected by turbulence and Lamont and Scott model was closer to their experimental results.

3.2 Planar Microfluidic Systems

The planar structure of microfluidic devices provides opportunities regarding compact design, affordable installation, small void volume, high surface area/volume ratio, and easy integration with several systems. Recently, with the advent of metal injection molding and bonding developments, the planar structure is commercialized [46]. Therefore, many studies have shown the utilization of planar structures to improve their performance with novel designs in various applications of industrial processes. Shellie et al. [46] devised a planar microfluidic device to employ it in a gas chromatography process for petrochemistry applications encompassing difficulties such as various boiling points of analytes. They developed different planar microfluidic devices with different selectivities. The microchannel they developed allowed high flow rates to prevent gas back diffusion and high-pressure drop. The planar system enhanced capillary gas chromatography efficiency.

Moreover, membrane fabrication methods with desired characteristics for planar applications are densely investigated because membrane integration to microfluidic systems has been still performed manually and challenging due to limited control of membrane fabrication and challenging membrane characteristics. For smaller dimensions, although desired characteristics of membranes can be obtained, porosity and surface area of membranes are relatively low [47]. Dubosc et al. [48] devised a system to fabricate a porous lateral silicon membrane that can be easily integrated into microfluidic structures for filtration processes. This study supports the implementation of lab-on-a-chip devices in medical applications more commonly. Similarly, He Y et al. [47] proposed a lateral silicon membrane fabrication method, which can be integrated into planar microfluidic systems. They successfully developed porous silicon membranes for planar microfluidic applications with desired pore location, size, and porosity, providing high versatility, although these membranes are more complex and expensive.

3.3 Membrane Technologies

A membrane can be defined as a permeable barrier between two different homogenous phases. Membrane applications have various advantages like obtaining more efficient and compact size devices, using a little number of chemicals, or facilitating automation-integrated systems. Membranes are classified based on various criteria, e.g., their pore diameter, shape, morphology, and separation processes. As membrane material, although synthetic polymers are mostly used, ceramic and metallic membranes are employed in some applications in the industry. The first known synthetic membrane was cellulosic and was employed in 1907. Generally, commercial production and usage of membranes date back to the early 1920s [49]. Currently, it is utilized in various sectors, which are mostly separation processes (gas, bacteria/virus, metal, and plasma). In these applications, membrane utilization would be costly because several membranes need to be consumed. Different applications may require unique membrane selection. For instance, PTFE is used if chemical resistance is necessary, or narrow size membranes are preferred to increase selectivity [50]. Regarding separation processes, the pore diameter of membranes is an essential characteristic as it changes the separation yield and selectivity of the membrane. It is categorized into four main groups according to pore diameter: reversible osmosis (up to 0.001 μm), nanofiltration (0.001-0.005 μm), ultrafiltration (0.005-0.05 μm), and microfiltration (0.05-2 μm), affecting membrane selectivity for different size particles to be separated [51].

Moreover, they are intensively facilitated in complicated microreactor technologies. Despite complicity, membrane integration into microfluidic devices has a novel architecture because immiscible fluids can be easily separated by using a porous membrane. Regarding membrane selection for these applications, water-repellent and breathability properties of membranes are significantly essential to design the most appropriate membrane-integrated microfluidic structure. Nonporous hydrophilic membranes or porous hydrophobic membranes can be employed to obtain waterproof and breathable devices. Mostly, hydrophobic membranes are preferred for these types of applications, offering many advantages and improving efficiencies. Several processes are issued in the literature, such as phase separation, mechanical stretching, and template-based method to prepare waterproof and breathable membranes [52].

3.3.1 Hydrophilic and Hydrophobic Membranes

Hydrophilicity or hydrophobicity of a membrane is a vital characteristic to adjust water or gas permeability, which has been extensively investigated. Therefore, employing a membrane with controlled hydrophilicity/ hydrophobicity is a primary focus [53]. To obtain a hydrophilic/hydrophobic membrane, we should consider the wetting properties of a membrane because hydrophilicity or hydrophobicity depends on these characteristics, affecting several properties of applications such as mass transfer resistance and absorption efficiency. Hydrophobic membranes are mostly preferable for gas venting processes. During operations of hydrophobic membrane-integrated devices, non-wetted (the most preferred because of minimum diffusion resistance through membrane' pores), partially-wetted or fully-wetted conditions may occur. Non-wetted systems are possible only in theoretical conditions for superhydrophobic membranes. In real conditions; however, hydrophobic membranes allow the intake of liquid phase into their capillaries to a certain degree. Various membrane features and operation parameters (porosity and liquid concentration) affect the degree of wetting; so, pores may be wetted either wholly or partially.

During operation, the wetness of the membrane increases gradually, leading to a decrease in mass transfer [54]. Lu et al. [55] investigated the wetting mechanism of hydrophobic membranes in mass transfer processes of gas absorption. According to the theoretical model they developed, contact angle, surface tension, and pore size distribution are important parameters for the wetting properties of the hydrophobic membrane. The contact angle between membrane surface and water droplets is significantly essential as it is a straightforward way to measure the hydrophobicity. A goniometer is used to measure the contact angle. To define a membrane as hydrophobic, the contact angle between the water droplet and membrane surface should be higher than 90˚. In this case, the surface energy of the membrane is lower, allowing the spherical shape of water droplets on the surface. If it is necessary to obtain superhydrophobic membranes, the contact angle needs to be maximized to a value greater than 150˚. Contact angle varies based on liquid structure (type or concentration) for a particular type of membrane [56]. Figure 3.1 represents the structure in idealized conditions, including sharp corners. In realistic conditions, the capillary has irregular shapes and smooth corners (in Figure 3.2) [57].

Regarding other parameters of the theoretical model in the paper belonged to Lu. et al. [55], increasing surface tension of aqueous solutions leads to slight wetting of membrane surfaces with high contact angles. This assumption may differ from the surfaces at low energy, like PTFE or polypropylene (PP) because of the non-wetting effects of some organic liquids with low surface tension [58]. Moreover, pore size and shapes are other significant criteria as these properties affect critical entry pressure that correlates liquid surface tension with contact angle. If a hydrophobic membrane has small cylindrical capillaries, curvature radii are accepted as constant, as demonstrated in Figure 3.1. Nevertheless, most membranes contain irregular pore shapes with angular curvatures shown in Figure 3.2, affecting critical entry.

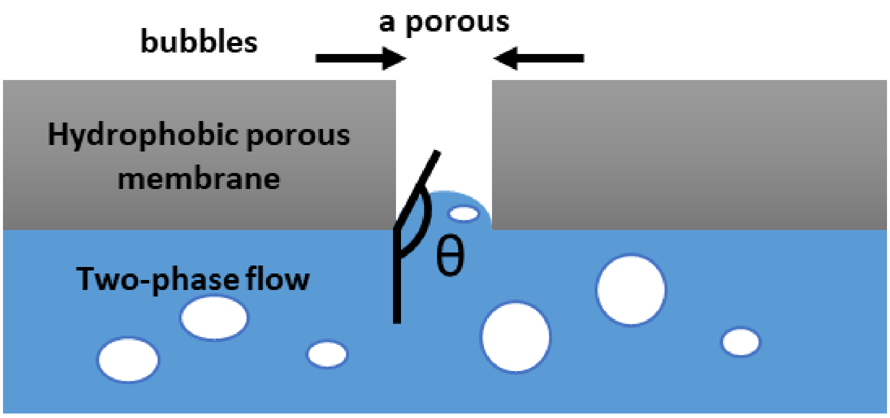

Figure 3.1 A pore in a hydrophobic membrane with a regular pore shape, preventing liquid leakage. θ illustrates the contact angle.

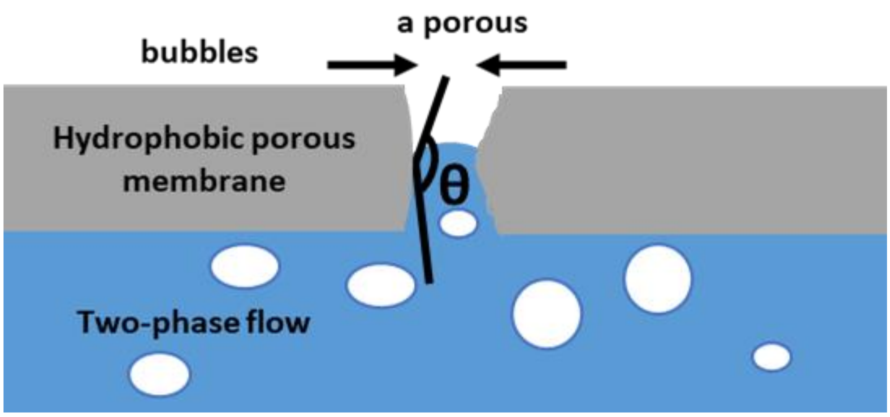

Figure 3.2 A pore in a hydrophobic membrane with an irregular pore shape, preventing liquid leakage. θ illustrates the contact angle.

3.3.2 Gas Permeability of Porous Hydrophobic Membranes

Another essential characteristic of the membranes employed for gas diffusion is its pore's permeability, depending on various factors like porosity, thickness, tortuosity, and operation temperature or the pressure difference across the membrane [59-61]. Gas permeability for this study is referred to as a gas transition through a rigid barrier. Permeability is a coefficient. Therefore, a theoretical equation can be derived to calculate various parameters. Mancy et al. developed an equation, correlating surface concentrations, membrane thickness, and gas flux indicated below [62]

$$q = k\frac{C_1 - C_2}{b} \tag{3.1}$$

where C_1 and C_2 represent surface concentrations, b is membrane thickness, q is gas flux, and k is referred to as permeability coefficient. One fluid transport model for membranes is the dusty model and can be represented below

$$\vartheta = \frac{k\Delta p}{\mu b} \tag{3.2}$$

where k is the membrane permeability, μ represents the fluid viscosity, b is the membrane thickness, Δp is pressure drop across the membrane, and ϑ is the fluid flow rate through the membrane. k varies according to pore size, porosity, and tortuosity (membrane properties), and can be calculated experimentally from equation 3.2. For some regular pore geometries; however, Hagen-Poiseuille (for cylindrical pores-equation 3.3), Richardson-Zaki (for flow through a bed of spherical particles- equation 3.4), and bed of fibers (3.5) equations can be theoretically applied.

$$k = \frac{d_p^2}{32} \tag{3.3}$$

$$k = \frac{d_p^2}{18}\varepsilon^{2.7} \tag{3.4}$$

$$k = \frac{d_P^2}{80}(\varepsilon^2/(1-\varepsilon)^2) \tag{3.5}$$

where d_p is pore diameter, and ε is the porosity of the suspension.

Regarding studies, Vundavilli et al. [63] investigated the bubble removal capacity of different hydrophobic PTFE membranes supplied from various companies, each of them has district characteristics in terms of pore size, porosity, structure material, and thickness. They evaluated the effects of various parameters (channel height, membrane properties, liquid flow rate) on bubble removal. The gas removal rate increased with the increase in pore size (as it increases the permeability) from 0.45 µm to 3 µm (Figure 3.4). However, it was necessary to select a pore size according to operating pressure that also depends on liquid breakthrough pressure. Therefore, 1-3 µm membrane pore size is appropriate when liquid breakthrough pressure is higher than 13 kPa. Generalized, increasing liquid flow rate; however, led to a decrease in the gas bubble removal since contact time between the gases and the membrane was reduced although the numerical values of gas flow rate (µl/min) also depend on the channel height and pore diameter. This implication was summarized in Figure 3.3 which is the gas diffusion rate through 1 µm hydrophobic membrane (Sterlitech) with respect to the liquid flow rate at various microfluidic channel heights. Moreover, this graph indicates that higher channel heights were more efficient for gas removal rate (µl/min).

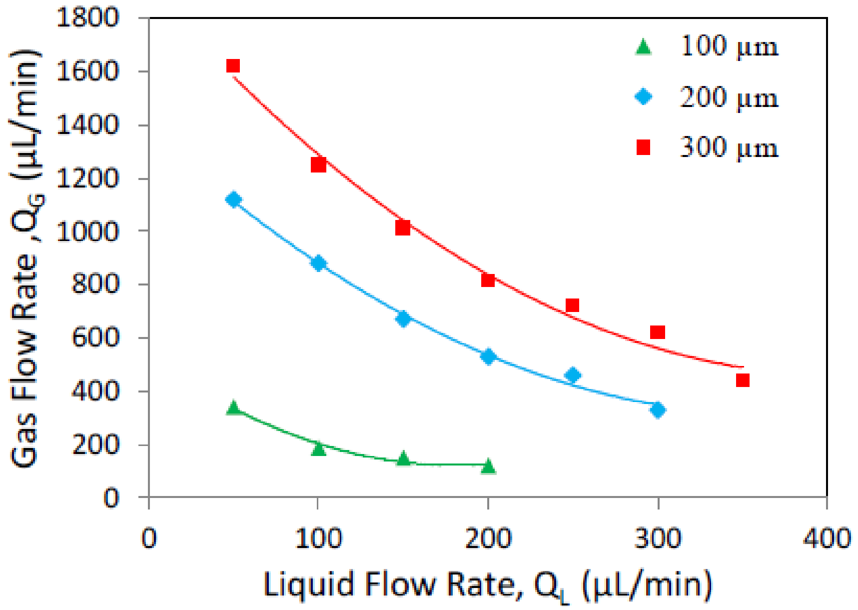

Figure 3.3 Gas bubble removal rate from 1 μm hydrophobic membrane (Sterlitech) at various channel heights and liquid flow rates [63].

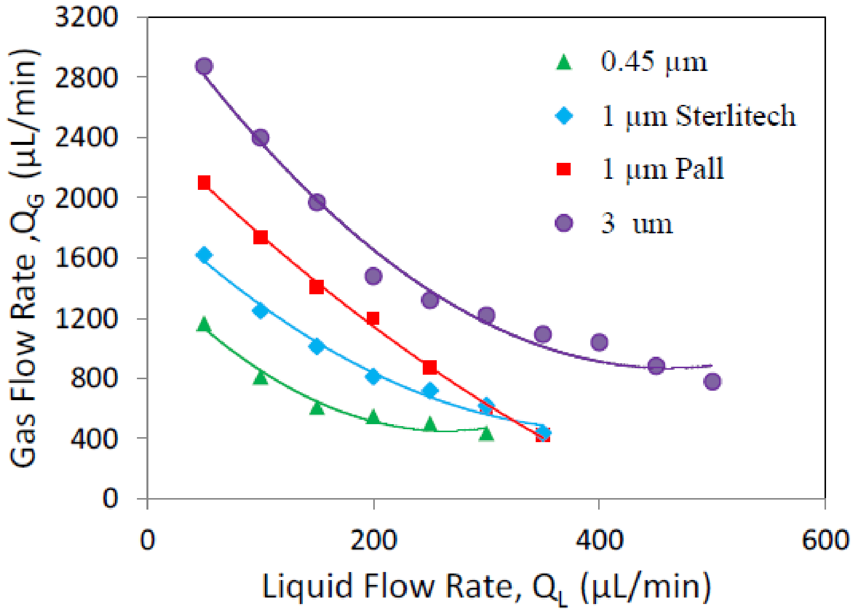

Figure 3.4 Gas bubble removal rate from different hydrophobic membranes at various pore diameters [63].

Kim H. et al. [61] calculated experimentally and theoretically, the mass transfer coefficients of PTFE membranes with different pore sizes which were 0.45 and 0.22 μm for membrane distillation applications. Mass transfer coefficient for PTFE membrane with 0.45 μm pore size was two times higher than that of PTFE membrane with 0.22 μm. Dobson et al. [62] calculated gas permeability coefficients of 6 μm PTFE membrane for different gases and compared these values with the literature. They observed a significant difference between their results and the literature, which may be caused by the various production processes of membranes.

3.4 Applications of Microfluidic Systems Integrated with Porous Membranes

Introducing porous layers into microfluidic devices has caught great attention since more efficient devices can be devised because of close contact between porous layers and microchannels. It is possible to design different microchannel geometries with various porous-structured layers. Hereijgers et al. [50] categorized these layers into the membrane, open tubular, disordered support, and ordered support layers. Among them, membrane layers have additional advantages regarding being thicker, involving small-pores and high porosity, and stabilizing the system. Therefore, integration of porous membranes into microfluidic systems is utilized in various fields of industry to improve their performance by affecting different features like pressure changes alongside microchannel, flow stabilities, and heat transfer coefficients. The rest of this section summarizes several studies regarding these novel systems.

Eddington et al. [64] combined a microfluidic chamber with a bubble trap to halt additional bubble growth through the chamber. However, this bubble trap stuck completely with bubbles after a certain point. Therefore, they offered an additional gas permeable PDMS membrane layer to wash out bubbles from the bubble trap. Although bubbles were successfully removed by applying positive pressure to the PDMS layer, one drawback was pausing the operation while removing bubbles through the PDMS layer. Skelley et al. [65]; however, presented a device including a bubble trap and de-bubbler, providing bubble removal without an experiment pause. Hence, they obtained the bubble-free system in a shorter time. David et al. [39] integrated a hydrophobic porous PTFE membrane into a parallel microchannel heat exchanger to improve the performance of non-venting heat exchangers by decreasing normalized pressure drop. For this purpose, they placed a porous hydrophobic membrane above the two-phase channel, transferring the bubble phase to the venting channel. This structure showed a 60 % improvement by decreasing the pressure drop through the channel. Meng et al. [57] performed a methanol fuel cell application by integrating hydrophobic membranes with a gas-venting anodic microchannel to solve the clogging and pressure drop problem. PTFE and PP membranes were utilized to constitute the microchannel. Accordingly, there was no leakage problem while utilizing the PP membrane, even at higher solution concentrations. Additionally, excessive power consumption was reduced. It can be attributed to that the gas phase was removed, and venting was successfully performed.

Crystallization separation is an important method for chemical engineering processes like purification. The types of equipment used in chemical engineering processes gave place to developing new microfluidic devices due to their advantages, although some common challenges for microfluidic devices remain. Timmer et al. [66] carried out an electrolyte concentration study in micro-sized evaporators by assembling a hydrophobic porous membrane to the evaporator. In this study, a micro-porous Teflon membrane was placed between the liquid solution and nitrogen carrier gas channels. This membrane allowed the transfer of water vapor from the liquid solution to the nitrogen flow region, and it was swept by flowing nitrogen gas. The restriction for this structure was the low removal rate of solvent, which applied to more volatile solvents. Therefore, He. et al. [67] performed a crystallization separation by introducing a laser-beam to a microfluidic evaporator embedded with a hydrophobic porous PTFE membrane. In this structure, they placed the membrane on top of the evaporation chamber, keeping the water droplet inside as the contact angle of the liquid phase was greater than 90 ˚. Infrared laser beam was continuously transmitted from the bottom of the chamber for the sudden increase of solution temperature, and then evaporation. Hence, solution concentration was increased until the dissolved solute was crystallized by removing the evaporated gas phases through a hydrophobic porous membrane.

One another field of applications for microfluidic systems integrated with porous membranes is the water treatment processes. Qasim et al. [68] integrated a nanofibrous hydrophilic membrane with a microfluidic device to obtain compact devices for these processes. Because of the advantages of nanoscale membranes utilizing the high surface area to volume ratio; porosity and filtration efficiency were significantly elevated. The microfluidic design they developed facilitated the integration process of the membrane to the microfluidic system by protecting its chemical and physical surface structure. They employed continuous flow and observed an efficiency increase from 60 % to 90 % with the integration of the membrane.

4
EXPERIMENTAL METHOD

4.1 Microfluidic Planar Water Electrolyzer Preparation

We designed and fabricated a planar microfluidic alkaline water electrolyzer. We used AutoCAD computer-aided program (CAD) to model the cell and made two-dimensional (2D) AutoCAD drawings while shaping the materials (polymethylmethacrylate (PMMA) and double-sided adhesive (DSA)) of some components of electrolyzers with a laser cutting because AutoCAD is easily compatible with a laser cutting machine. A schematic diagram of the membraneless planar microfluidic water electrolyzer can be seen in Figure 4.1. The bulk dimensions of the electrolyzer were 40 mm x 40 mm x 10 mm, while the microfluidic chamber thickness was 400 μm. The main components forming the microfluidic chamber were PMMA and DSA layers. A non-conductive 5 mm PMMA film was used as the top and the bottom layers of the electrolyzer due to its easy processability. The base and the top PMMA layers were bound to each other with the help of a 400 μm DSA that was cut into a similar shape to PMMA. 1 cm x 3 cm thin nickel (Ni) plate electrodes were placed on both sides of the bottom DSA layer positioning on the PMMA layer. The distance between the electrodes was 2 mm. The PMMA layer was placed on the top, containing one inlet and two outlets, allowing the flowing streams of the electrolyte separately. Furthermore, the electrolyzer was sandwiched between two stainless steel layers with screws to prevent leaking of the electrolyte from the sides. Another electrolyzer structure we proposed included the embedment of a hydrophobic porous membrane under the top PMMA layer that has an opening to allow gas removal. The membrane layer embedded in the electrolyzer was wider compared to the top PMMA opening to prevent air passage through the edges. This membrane was purchased from Sterlitech, and its specifications can be found in Table 4.1.

Except for the top PMMA layer opening and membrane embedment, other components' materials and dimensions were completely as same as the membraneless electrolyzer. Figure 4.2 indicates a schematic diagram of this membrane-embedded structure.

Table 4.1 Specifications of PTFE unlaminated membrane filters.

Supplier	Pore Size µm	Diameter mm	Support Material	Thickness µm	Water Entry Pressure psi
Sterlitech	1.0	47	Unsupported	203-305	5.5-6.5

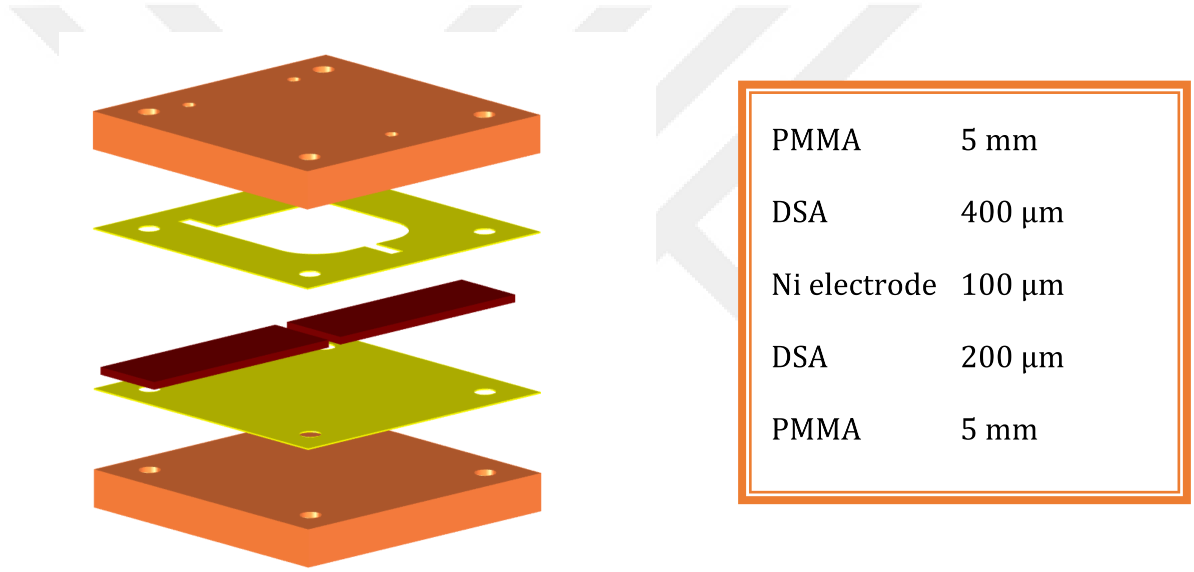

Figure 4.1 A schematic diagram of the membraneless planar water electrolyzer with layers and thicknesses.

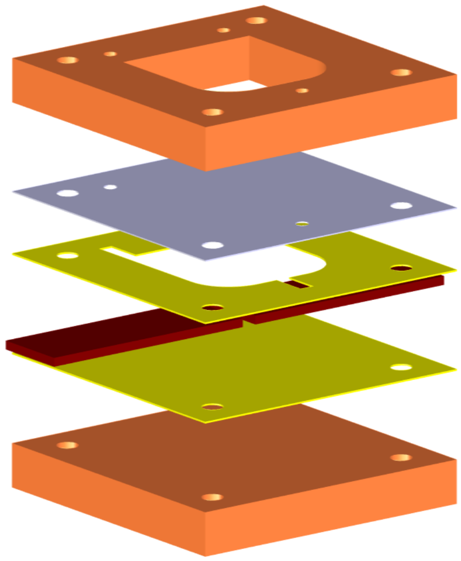

PMMA	5 mm
Membrane	203-305 µm
DSA	400 µm
Ni electrode	100 µm
DSA	200 µm
PMMA	5 mm

Figure 4.2 A schematic diagram of the membrane-embedded planar water electrolyzer with layers and thicknesses.

4.2 Electrode and Electrolyte Preparation

100 µm thick pure Ni plate whose dimensions were 500 mm x 30 mm was cut into the pieces that were 30 mm x 10 mm by using the wire erosion machine to obtain electrodes. The last stage was the treatment of each piece for 240 seconds with a 0.25 µ Aqua-Pol Diamond Suspension solution as abrasive with the help of a Minitech 233 polishing device. The rotation speed of the device was 50 rpm. KOH pellets (1.05012.1000 EMPLURA) were purchased from Merck, and 2 M KOH solution was prepared as the electrolyte.

4.3 Experimental Setup

The electrolyte was stored in the 100 ml autoclave glass consisting of two openings in the lid to accommodate hoses. One hose was conveying air into the glass storage, supplying a pressure to initiate electrolyte flow at the adjusted flow rate of the syringe pump. Another hose was pumping the electrolyte to the electrolyzer. A hot plate was placed under the glass storage to keep the temperature constant as 25 ˚C, 40 ˚C, and 65 ˚C during electrolysis experiments. When the device was fabricated firstly, it was tested against the possibility of leakage and obstructions by preserving water as the electrolyte instead of KOH solution. In Figures 4.3.a and 4.3.b, cross-sectional view of the microfluidic chamber and the working mechanism of the electrolyzers can be seen for the membraneless and membrane-embedded electrolyzers, respectively. Moreover, Figures 4.4, 4.5, and 4.6 represent the picture of the membrane-embedded cell and a cross-sectional view of electrolyzers as well as a schematic drawing and a picture of the experimental set-up.

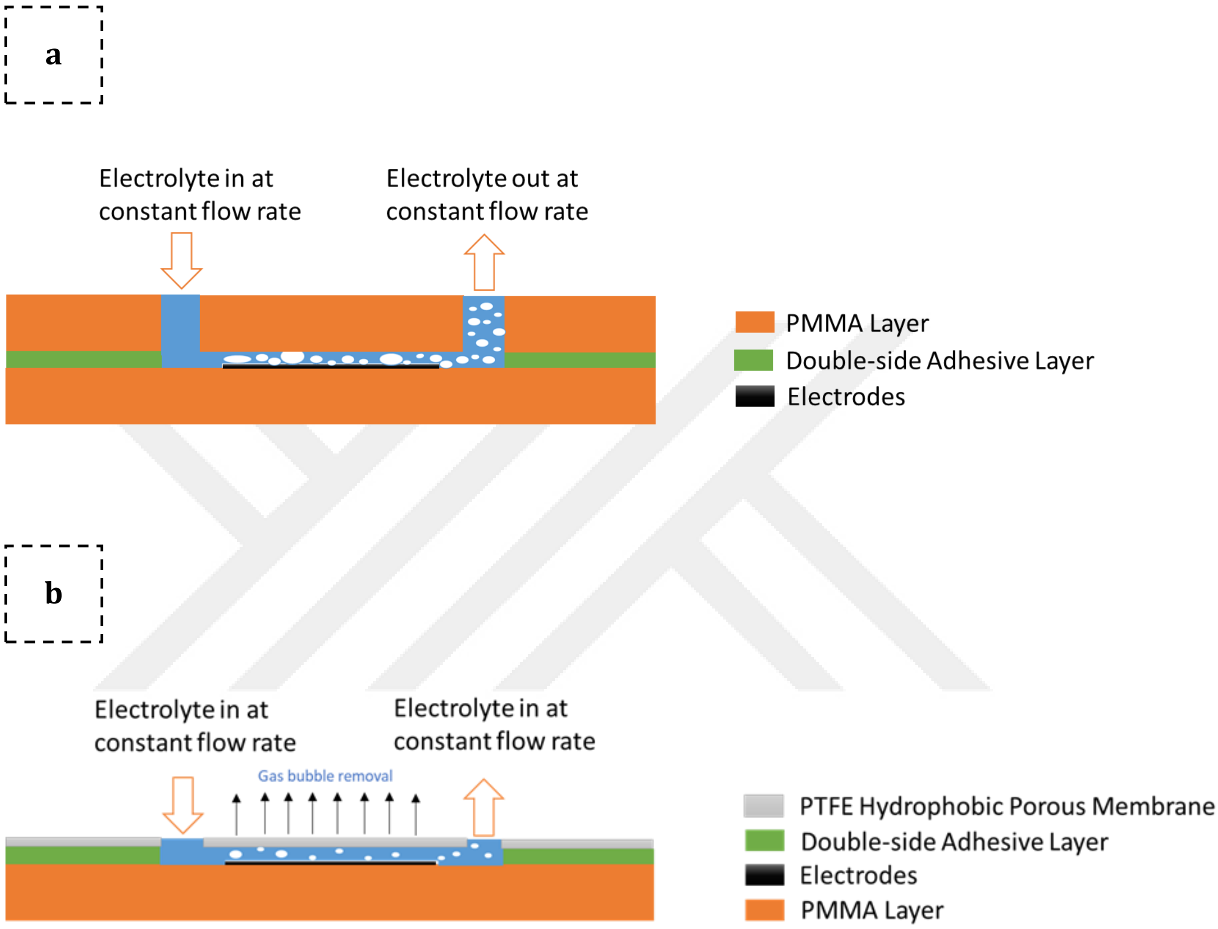

Figure 4.3 The electrolyzer working mechanism and a side view of the microfluidic chamber **a)** in the membraneless electrolyzer. **b)** in the membrane-embedded electrolyzer.

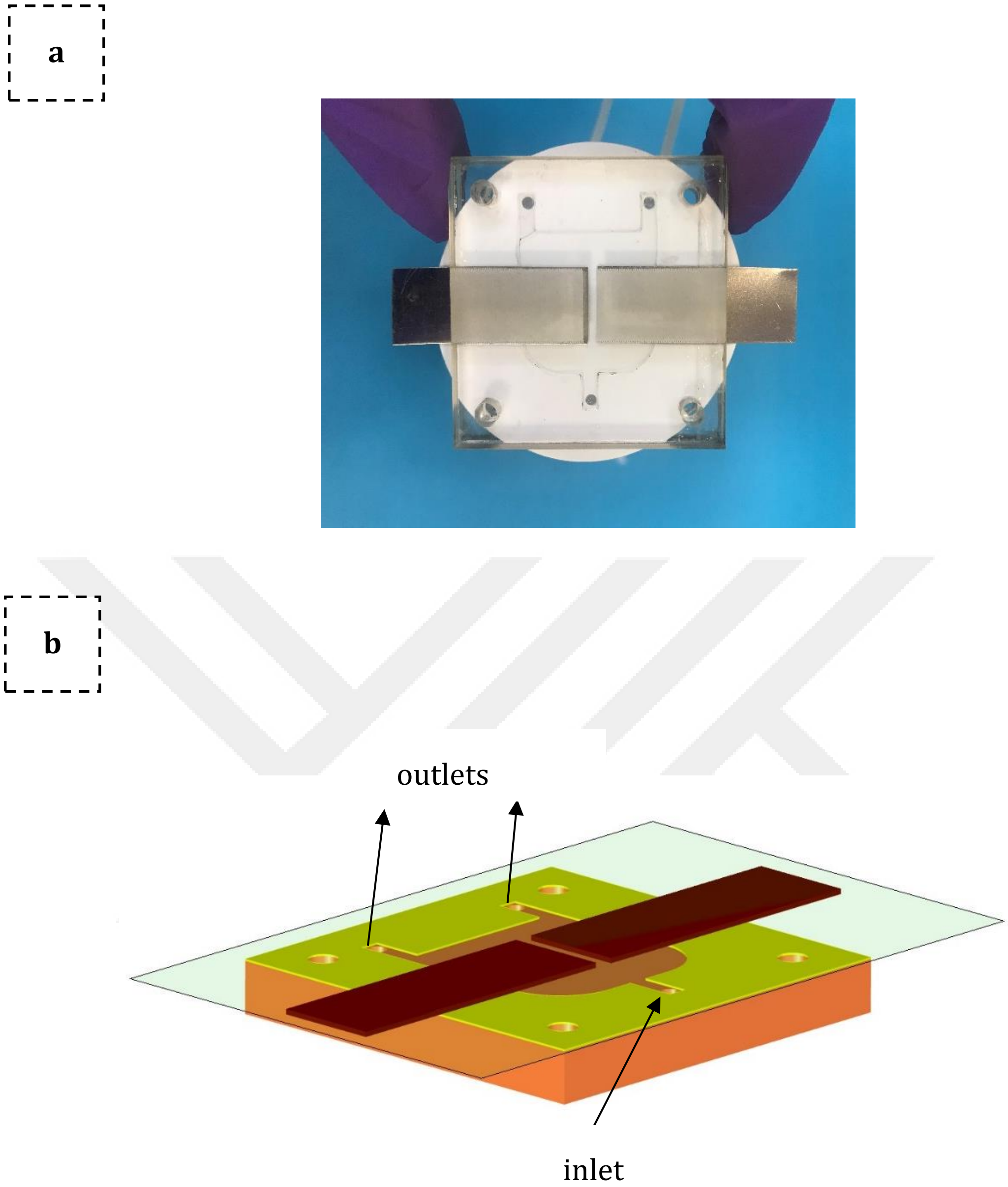

Figure 4.4 a) The membrane-embedded water electrolyzer cell. 40 mm x 40 mm PMMA layer, 1 cm^2 electrode area for each electrode, and 400 μm chamber height (The picture was taken from the bottom side) **b)** a cross-sectional view of the planar electrolyzers.

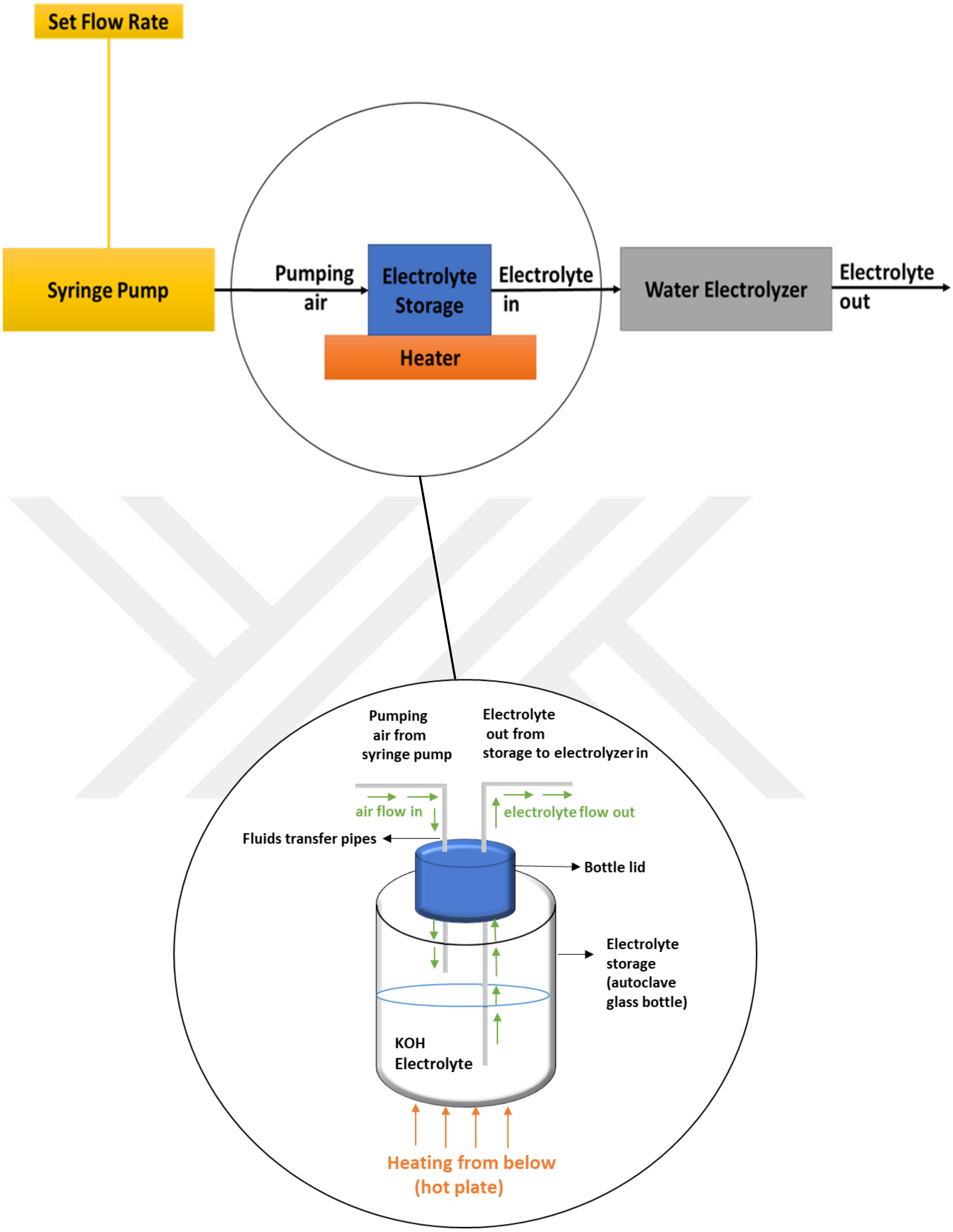

Figure 4.5 A schematic diagram of the experimental set-up and flow system.

Figure 4.6 Picture of the experimental set-up.

4.4 Electrochemical Measurements

Ivium CompactStat instrument was employed to conduct electrochemical measurements. 2-electrode configuration of the electrochemical experiments was carried out. The working electrode (WE) and the sense electrode (S) were plugged into each other. The same was conducted for the counter electrode (CE) and the reference electrode (RE) to connect electrodes according to the 2-electrode electrochemical configuration. Electrodes were connected to the positive and negative poles of the potentiostat. Ground connection (G) was placed in a shielding body to reduce noise. Theoretically, while carrying current is performed by the WE and CE, the RE and S measure the potential. The control loop of the instrument applies a signal to CE. After cable connections are completed, an appropriate measurement technique is selected from the software of the IviumStat. We selected chronoamperometry mode for constant current measurements to record currents from the transients bar on the method section. We changed the applied potentials as 1.8 V, 2.0 V, and 2.2 V and interval time as 0.2 s manually. Moreover, auto-current mode was selected with 100 A maximum range and 100 nA minimum range.

Chronopotentiometry mode was selected for constant voltage measurements to record the voltage. The potential range was 4 V and constant current densities were 0.6 mA/cm^2 and 1.7 mA/cm^2.

The numerical values of current versus time graphs were used to calculate the amount of hydrogen that is produced, and voltage versus time graphs were employed to calculate electrochemical efficiencies during electrolysis at selected conditions and different configurations. We utilized the equations represented below to calculate the amounts of hydrogen produced from the chronoamperometry mode.

The quantity of electric charge is associated with one mole of electrons. It is provided by Faraday constant, which is represented below

$$1\, mol\, e^- = 96485\, C \tag{4.1}$$

Electric charge is not measured directly. Instead, electric current (A) is measured, which represents the passage of 1 coulomb of charge per second (C/s).

$$charge\ (C) = current\ (C/s).\, time\ (s) \tag{4.2}$$

where C is the total quantity of charge transferred. The number of moles of electrons involves in an electrolysis reaction is represented below

$$number\ of\ mole\ e^- = current\ (C/s)\ x\ time\ (s)\ x\ \frac{1\, mol\, e^-}{96485\, C} \tag{4.3}$$

Based on cathode half-reaction (Equation 2.2) of water electrolysis, 2 moles of electrons are involved to produce 1 mol of hydrogen. Therefore, 2 moles of electrons yields 1 mol hydrogen gas at standard temperature and pressure [69].

5
RESULTS AND DISCUSSION

5.1 Introduction

Gas management is a critical issue in microfluidics for the efficient operation of electrolyzers. Gas bubbles inevitably form, and they cover the electrode surface during electrolysis, reducing the available electrode surface area for heat and mass transfer between electrolyte and electrode surface. Different ways have been conducted to overcome this challenge [70, 71]. One of them is using gas-permeable porous membranes, and it would be an efficient way. Therefore, integration of the membranes to hydrogen-producing devices has received significant interest.

We demonstrated this approach on a microfluidic planar alkaline water electrolyzer; thus, we proposed a new electrolyzer design including a porous hydrophobic membrane and compared the performance of this electrolyzer with a membraneless version at various operating conditions. These electrolyzers we proposed verified by adjusting operating conditions, such as flow rate, temperature, and applied potential, and by comparing them with theoretical situations. To test the effects of operating conditions on hydrogen production performance, we carried out experiments at constant voltage and at constant current by recording currents as a unit of milliamperes (mA) and voltages as a unit of volts (V), respectively. By applying constant voltage, we ascertained how flow rate, temperature, and applied cell potential affect our electrolyzers' performance; then, we selected optimum operating conditions. With the help of constant current experiments, we compared the energetic efficiencies of the membrane-embedded and membraneless electrolyzers to understand whether assembling the hydrophobic porous membrane to our design would work. The amounts of hydrogen produced and the energetic efficiencies of the electrolyzers successfully increased with the integration of the hydrophobic membranes. Recorded and calculated values supported our hypothesis in terms of the rapid gas removal through the pores of the membranes and addressing of the blockage problem in microchannels.

5.2 Design of a Water Electrolyzer and Selection of Operating Parameters

We aimed to achieve a gas bubble-reduced microfluidic planar water electrolyzers regardless of their applications by integrating a gas-permeable membrane into a microfluidic electrolyzer. Therefore, we designed the components of electrolyzers and selected operating parameters to observe rapid gas removal thanks to porous hydrophobic membrane integration, increasing the hydrogen amount produced and hydrogen production efficiency. Particular interest was required for the proper design of each component. We focused primarily on the electrolysis chamber (materials and dimensions); material selection, and positioning and integration of components while assembling the electrolyzer. One of the essential points was to design the electrolysis chamber. The electrolysis chamber should permit a steady flow of the electrolyte and the collection of H_2 and O_2 separately to prevent a dangerous mixture of them. An electrolyte membrane was not used because of the planar chamber design, allowing a separate flow of streams of H_2 and O_2. PMMA and DSA layers were used to constitute the microfluidic chamber, containing one inlet and two outlets at the top layer. The reason why we selected the PMMA was that it could be found easily and processed quickly with different methods; e.g. laser cut.

Regarding electrolyte, KOH and NaOH solutions are mostly preferred in the current alkaline water electrolyzers. Potassium ions (K^+) have higher ionic conductivity, resulting in less electric consumption [72] and mobility than sodium ions (Na^+) [73]. Therefore, a 2 M KOH solution was employed as an electrolyte. Although 6 M KOH solution is generally employed during alkaline water electrolysis, we selected 2 M KOH solution since our primary approach was to compare two different systems to observe hydrophobic porous membrane effects on the amounts of hydrogen produced and overall electrolysis efficiency and to investigate the employability of the membrane that we selected in future studies.

Pure Ni was selected as the electrode for the cathode and the anode since Ni is not only affordable but also stable metal for alkaline water electrolyzers. Besides, nickel is resistant to corrosion of the alkaline solutions, especially to KOH solutions [74]. We polished Ni electrodes to remove impurities, leading to a more available active area for the electrochemical reactions as well as to obtain smoother electrode surfaces since smoother electrodes provide equal Ni surfaces area for electrochemical activities to compare the effects of membrane utilization and operating parameters.

Regarding positioning, the distance between the electrodes of the cathode and anode was an essential criterion because cell resistance can be decreased while keeping the electrodes close to each other. Therefore, we kept the distance as close as possible. Nevertheless, it was not a zero-gap system, and a distance was necessary to flow of H_2 and O_2 streams without mixing due to lack of diaphragm.

Additionally, we conducted the experiments at various temperatures, flow rates, and cell potentials to determine optimum operating parameters for the most efficient design in both constant voltage and constant current measurements. The primary situation to be considered was to ensure the same operating conditions at the membrane-embedded and membraneless electrolyzers to select the appropriate parameters precisely.

At the membrane embedment stage, the main difference was a gap in the roof PMMA layer, allowing the removal of gases, coming from the porous hydrophobic PTFE membrane. We selected the membrane based on its hydrophobicity, pore size, and thickness. Because of its hydrophobic structure, no liquid escapes through the membrane due to surface tension forces, enabling only gas transition out. As liquid cannot go into the pores of the membrane, water can flow under the membrane barrier until water entry pressure of the membrane. It is expected to rise the gas removal rate with the increase of the pore size as indicated in Figure 3.4, representing pore size and gas diffusion rate relation [63]. Moreover, if thin membranes were used, membrane assembling would create problems [20]. Therefore, we selected a relatively thick membrane for our design, which was SterliTech PTFE unlaminated membrane filters. Specifications of this membrane can be found in Table 4.1 in the fourth chapter of this thesis.

5.3 Constant Voltage Measurements

We performed electrolysis at various constant voltages to record currents at different operating flow rates and temperatures as a function of time. By evaluating the current-time graphs obtained from the Ivium software, we deduced how temperature, flow rate, and applied potential, as well as the hydrophobic porous membrane, affect our electrolyzer performance. The current data indicated in Figures 5.1 through 5.7 were recorded for 0.9 cm^2 cathode electrode surface area.

5.3.1 Hydrophobic Porous Membrane Usage

All electrolyzers have main common drawbacks regardless of their acidic or basic structure. One of them is the forming and releasing of gas bubbles, causing bubble overpotentials [15] that receive great attention to overcome. Another drawback is using an ion-permeable membrane between the anode and cathode to prevent the mixing of H_2 and O_2. Clogging of a microfluidic channel with gas bubbles causes a decrease of the active surface area of the electrodes, limiting heat and mass transfers. To defeat these limitations and to improve hydrogen production efficiency, we embedded a hydrophobic membrane to our electrolyzer design in order to remove gas bubbles rapidly and obtain a more available active site on the electrode surface. In a two-phase flow, the vapor phase adds extra friction to the flow [39]. By separating the vapor phase with the help of the hydrophobic membrane, a more consistent flow rate can be obtained alongside the microfluidic channel. The reason why we selected a PTFE hydrophobic membrane was to create a device providing no leakage out of the device. Because, PTFE membrane we used was extremely hydrophobic, and this structure kept the liquid electrolyte inside of the chamber although flowing electrolyte put pressure on the above membrane layer until the water entry pressure was 5.5-6.5 psi. They were produced through a process, bringing significant properties to these chemically and biologically inert membranes, some of which are high porosity, uniform thickness, and thermostability up to 260 °C. With these characteristics, they can be used in the process of gas removal, including water vapor and hydrogen and oxygen gas bubbles. No leakage problem at our experimental conditions tested claims regarding its features. Experiment conditions were kept the same for the membrane-embedded and membraneless electrolyzers to realize the effects of the hydrophobic membrane. Parameters were selected 1.8 V, 2.0 V, and 2.2 V as cell potentials; 25 ˚C, 40 ˚C, and 65 ˚C as temperatures and 5 ml/min and 1 ml/min as flow rates. For all experiment sets, overall hydrogen production rates in the membrane-embedded electrolyzers were higher than those in the membraneless electrolyzers at the same operating conditions. Figures 5.1, 5.2, and 5.3 demonstrate recorded currents (mA) as a function of time at the flow rate of 1 ml/min and the temperatures of 25 ˚C, 65 ˚C. The fixed electrolysis cell voltages are 1.8 V, 2.0 V, and 2.2 V, respectively. At all applied voltages, Figures 5.1, 5.2, and 5.3 affirmed that membrane-embedded electrolyzers yielded more hydrogen than that of membraneless ones. According to Figure 5.3 (electrolysis at 2.2 V), the results at the temperature of 25 ˚C in the membrane-embedded electrolyzer showed improved performance than the results at 65 ˚C in the electrolyzer without membrane. Therefore, we can say that the membrane-embedded electrolyzers operating at the lower temperature would be more efficient than membraneless electrolyzers operating at higher temperatures, and assembling the membrane worked efficiently.

Although usage of the gas-permeable membrane would be an efficient way to decrease gas bubble clogging of a microchannel, Sung et al. [75] stated that gas removal rates in practical applications are relatively low until a certain point. Therefore, it was necessary to allow appropriate time for the system to balance. In Figure 5.1, 5.2, and 5.3, approximately 30 to 40 seconds passed until obtaining more consistent results at 1.8 V, 2.0 V, and 2.2 V applied cell voltages, which was valid in both membrane-embedded and membraneless electrolyzers.

Table 5.1 and Table 5.2 represent the ratios of total hydrogen amounts in the membrane-embedded electrolyzer to those in the membraneless electrolyzer during 1-hour of electrolysis at all experimental applied voltages (1.8 V, 2.0 V, 2.2 V) and temperatures (25 ˚C, 40 ˚C, 65 ˚C) for the flow rates of 5 ml/min and 1 ml/min, respectively. The ratios were more than one at all operating parameters of temperature, applied potential, and flow rate. Therefore, we can say that the embedment of the hydrophobic membrane worked properly and improved the efficiency of the electrolyzers. Moreover, these ratios were smaller at the flow rate of 5 ml/min compared to the ratios of 1 ml/min flow rate. This can be attributed to that gas bubbles (especially at higher temperatures and voltages) in the microchannels were removed with the help of higher flow rates, increasing the performance of the membraneless electrolyzer. When the flow rate was decreased to 1 ml/min, the microchannels in the membraneless electrolyzer were prone to clog, limiting the amount of hydrogen production; however, the membrane-embedded electrolyzer efficiently performed since it allows rapid gas removal from its pores, even at a lower flow rate (1 ml/min).

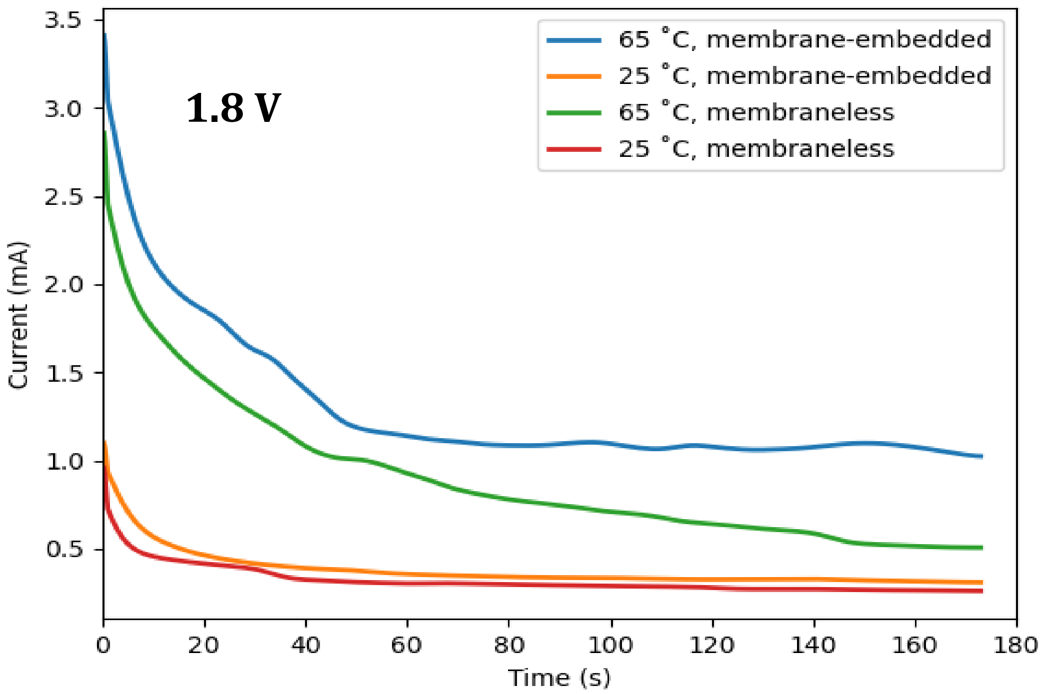

Figure 5.1 The hydrogen production currents for the electrolyzers with and without hydrophobic membrane at the flow rate of 1 ml/min and the potential of 1.8 V in the electrolyte of 2 M KOH.

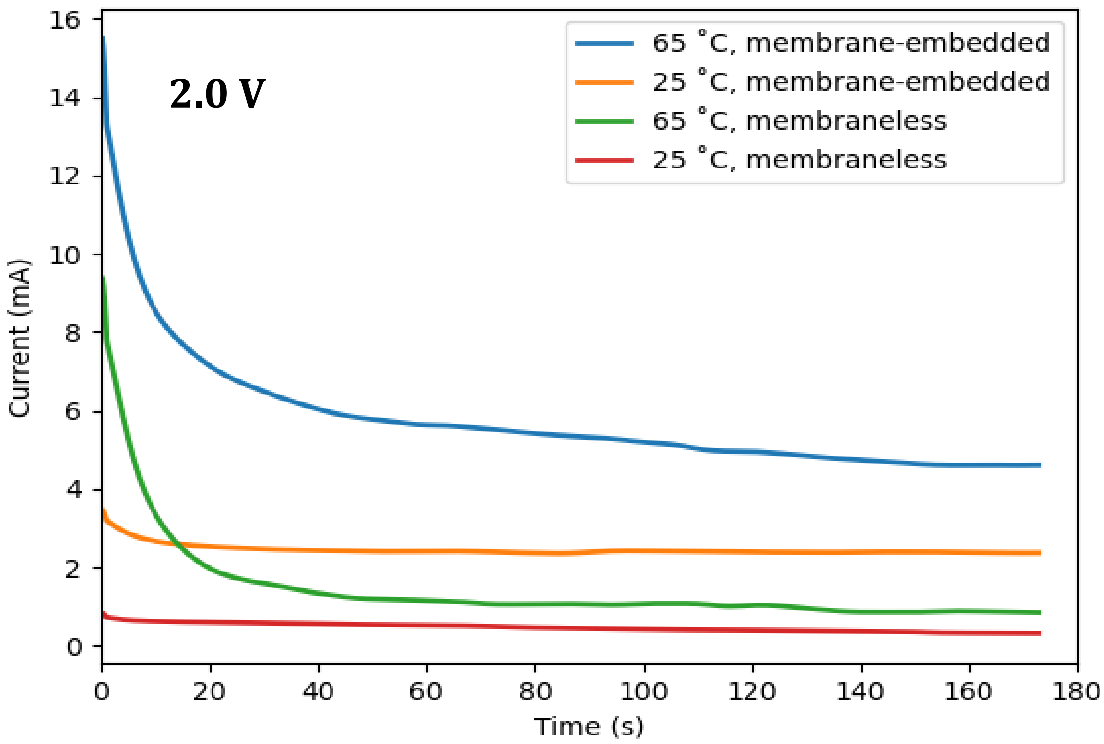

Figure 5.2 The hydrogen production currents for the electrolyzers with and without hydrophobic membrane at the flow rate of 1 ml/min and at the potential of 2.0 V in the electrolyte of 2 M KOH.

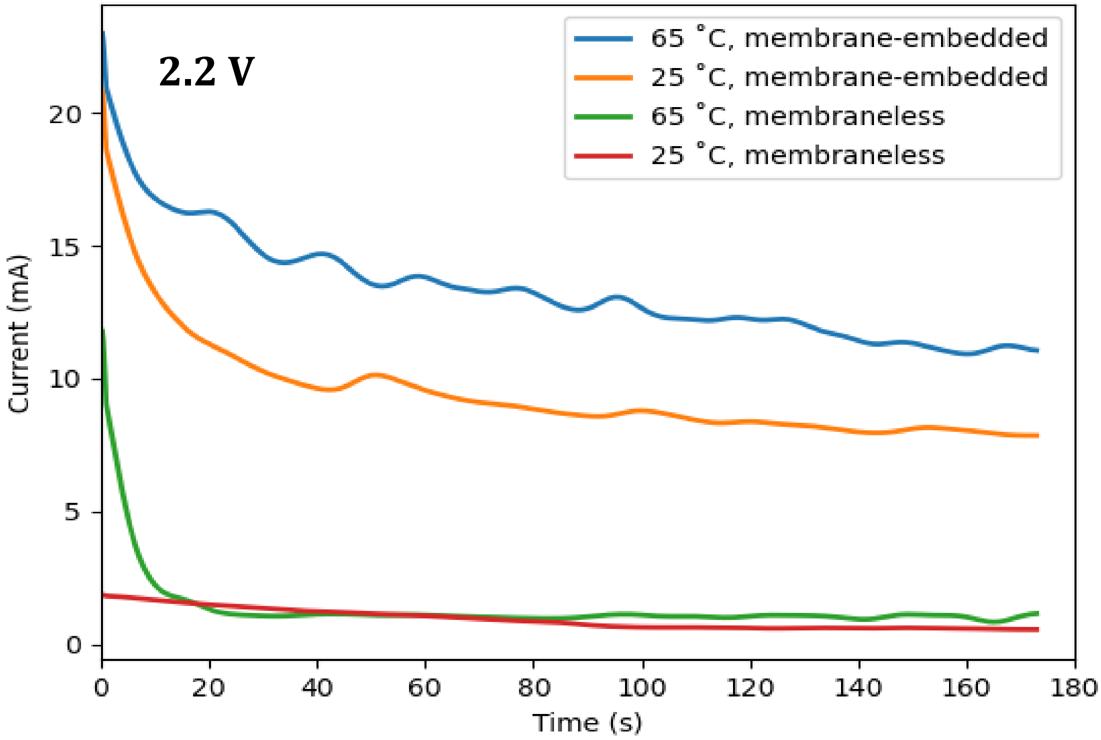

Figure 5.3 The hydrogen production currents for the electrolyzers with and without hydrophobic membrane at the flow rate of 1 ml/min and at the potential of 2.2 V in the electrolyte of 2 M KOH.

Table 5.1 The ratio of total hydrogen produced during 1-hour electrolysis in membrane-embedded electrolyzer to those in membraneless electrolyzer at the cell potential of 1.8 V, 2.0 V, 2.2 V and at the temperatures of 25 ˚C, 40 ˚C and 65 ˚C for 5 ml/min electrolyte flow rate pumping in the electrolyzer.

	@ 25 ˚C	**@ 40 ˚C**	**@ 65 ˚ C**
@ 1.8 V	2.21	2.23	2.61
@ 2.0 V	4.04	2.68	2.74
@ 2.2 V	12.24	4.50	4.16

Table 5.2 The ratio of total hydrogen produced during 1-hour electrolysis in membrane-embedded electrolyzer to those in membraneless electrolyzer at the cell potential of 1.8 V, 2.0 V, 2.2 V, and at the temperatures of 25 ˚C, 40 ˚C and 65 ˚C for 1 ml/min electrolyte flow rate pumping in the electrolyzer.

	@ 25 ˚C	**@ 40 ˚C**	**@ 65 ˚ C**
@ 1.8 V	1.17	2.17	1.65
@ 2.0 V	6.09	5.54	5.12
@ 2.2 V	12.25	15.05	11.77

5.3.2 Effects of the Parameters on Efficiency of the Hydrogen Production

5.3.2.1 Flow Rate

It was required to validate how operating parameters affect our electrolyzer efficiency to prove whether our design coincides with the literature and working principles of the commercial electrolyzers. Gas bubbles removal from the electrode surface was our primary focus, which was mitigation to increase the overall electrolyzer efficiencies. Experiments were carried out at the flow rates of 5 ml/min and 1 ml/min for the membrane-embedded and membraneless electrolyzers to understand the effects of electrolyte flow rate pumping into the electrolyzer. Laminar flow was achieved to prevent a hazardous mixture of hydrogen and oxygen gases because of the possible Vortex taking place on the turbulent flow [7]. Moreover, laminar flow ensures a parallel flow of the H_2 and O_2 streams through the micro-size channel. Hence, no physical component was necessary to separate them.

Vundavilli et al. [63] indicated that bubble diffusion rate through membrane pores increases with the decreasing of the liquid flow rate since contact time between the gas phase and porous membrane increases, leading to efficient gas removal. On the other hand, Vogt et al. [76, 77] stated that flow rate affects the gas density over the electrode when the electrolyte flows parallel to the electrode surface, concluding that gas density decreased with higher flow rate because of easy gas bubbles detachment from the electrode surface.

Figures 5.4 and 5.5 depict the recorded currents as a unit of milliamperes (mA) versus time at the voltage of 2.0 V, at the temperature of 25 ˚C and 65 ˚C, and the flow rates of 5 ml/min and 1 ml/min for the membraneless and membrane-embedded electrolyzers, respectively. It is easy to observe the flow rate characteristic of our electrolyzers with these two figures. The results have indicated hydrogen production rates decreased in time, which means that gas bubbles were evolved and stuck in the microchannel. According to the results, current densities; so, hydrogen production amounts, were higher when the operating flow rate was increased from 1 ml/min to 5 ml/min in the membrane-embedded and membraneless designs. Therefore, we can say that higher operating flow rates were advantageous to detach gas bubbles forming on the electrode surface as Vogt. et al.

stated; hence, full of bubble coverage on the electrode surface was prevented, which ensures more available electrode surface area for the electrochemical reaction. Measurements at the 1.8 V and 2.2 V cell potentials also supported this implication at all temperatures, which were 25 ˚C, 40 ˚C, and 65 ˚C.

Another important factor for the electrolysis reaction rate was the contact time between the electrolyte and electrodes. It declines when the flow rate is increased. For our case, hydrogen production was not high at lower operating flow rates; even the electrolyte temperature was increased to 65 ˚C. The selection of the optimum flow rate depends on the intended purpose of the electrolyzer. For instance, for microfluidic electrolyzers integrated with a thermal source like photovoltaics, the contact time of the control volume of the electrolyte in the microfluidic chamber is an important parameter, providing more interaction between the electrolyte and thermal source at lower flow rates. In this case, lower flow rates may have advantages to benefit from the thermal source. However, we assumed the steady-state of the electrolyte temperature at each point in the microchannel during the electrolysis, and there was no additional thermal energy source to heat the electrolyte within the electrolyzer. Therefore, contact time was not an essential criterion for us, and we could observe the direct proportion between the operating flow rate and hydrogen production efficiency.

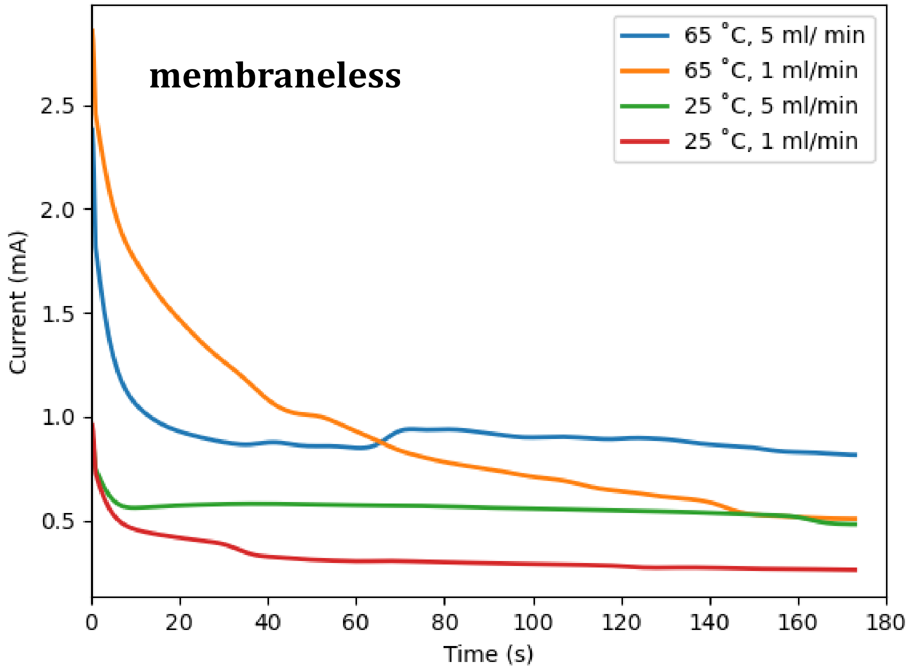

Figure 5.4 The effect of flow rate on the hydrogen production at the temperature of 25 ˚C and 65 ˚C at the potential of 1.8 V in the electrolyte of 2 M KOH.

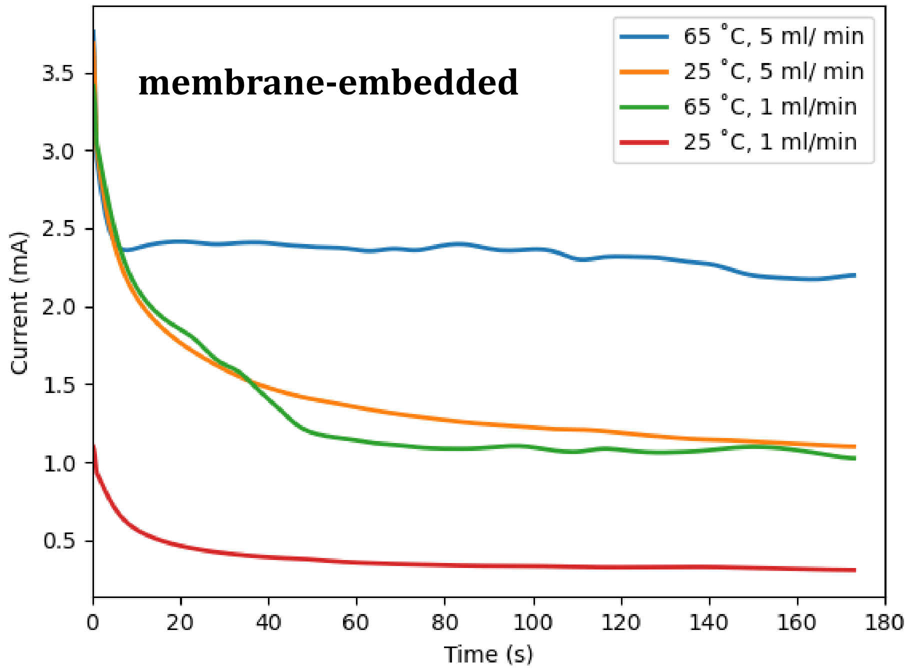

Figure 5.5 The effect of flow rate on the hydrogen production at the temperature of 25 ˚C and 65 ˚C at the potential of 1.8 V in the electrolyte of 2 M KOH.

5.3.2.2 Temperature

We wanted to observe the current-temperature relationship for our electrolyzers at the constant cell potentials and fixed electrolyte flow rate by carrying out the experiments at different temperatures of 25 ˚C, 40 ˚C, and 65 ˚C. We adjusted the constant electrolyte temperature during electrolysis by placing a hot plate under the electrolyte storage.

Figures 5.6 and Figure 5.7 depict the numerical values of recorded currents (mA) as a function of time (s) at the flow rates of 5 ml/min and applied voltages of 2.0 V for the membraneless and membrane-embedded electrolyzers, respectively. Hydrogen production increased with the increase in the temperature for both electrolyzers. This expected increase was valid for the experimental sets at 1.8 V and 2.2 V applied potentials and 1 ml/min operating flow rates. Because higher operating temperatures reduce the overpotentials on the electrode surfaces; so, accelerate the kinetics of the reaction, and generate more hydrogen, yielding more efficient electrolyzers.

Electrolyte conductivity is another significant feature affected by temperature changes. Stojic et al. [72] demonstrated that electrolyte solution conductivity was proportional to electrolyte temperature. We obtained similar hydrogen production patterns for different operating temperatures regardless of the addition of the hydrophobic membrane, which is shown in Figures 5.6 and 5.7. The only effect of the membrane embedment at this point was that higher amounts of hydrogen were obtained from the membrane-embedded electrolyzers. Additionally, Figures 5.6 and 5.7 indicate that more fluctuations were observed at higher temperatures of the membraneless electrolyzer at the flow rate of 5 ml/min. This pattern can be attributed to that gas bubbles could be removed at intervals for the membraneless electrolyzers operating at higher flow rates due to intense gas accumulation (no consistent removal). Under identical conditions; however, smoother patterns were obtained from the membrane-embedded electrolyzers in that consistent bubble removal could be achieved alongside the microchannel thanks to simultaneous gas removal from the pores of the hydrophobic membrane. Thus, we proved that higher electrolysis temperatures enhance the energetic hydrogen production efficiencies of membrane-embedded electrolyzers and believe that the working principle of our electrolyzers complied with the general concepts of commercial water electrolyzers regarding temperature. However, it should be taken into consideration that similar performance may be achieved for electrolyzers operating at lower temperatures or higher temperatures with the help of different novel innovations [78]. In our case, offering the hydrophobic porous membrane embedment supports achieving an almost similar performance from the membrane-embedded electrolyzer operating at lower temperatures like 25 ˚C with those from the membraneless electrolyzer operating at 40 ˚C.

Moreover, a decrease of current taking place in the last 20 seconds even for the membrane-embedded systems were acceptable since gas bubble accumulations may occur in time. Sweeping of them was required at intervals by transferring the electrolyte at high flow rates until the maximum pressure limit to detach sticking bubbles on the electrode surface (5.5-6.5 psi for the membrane we used, to prevent leakage).

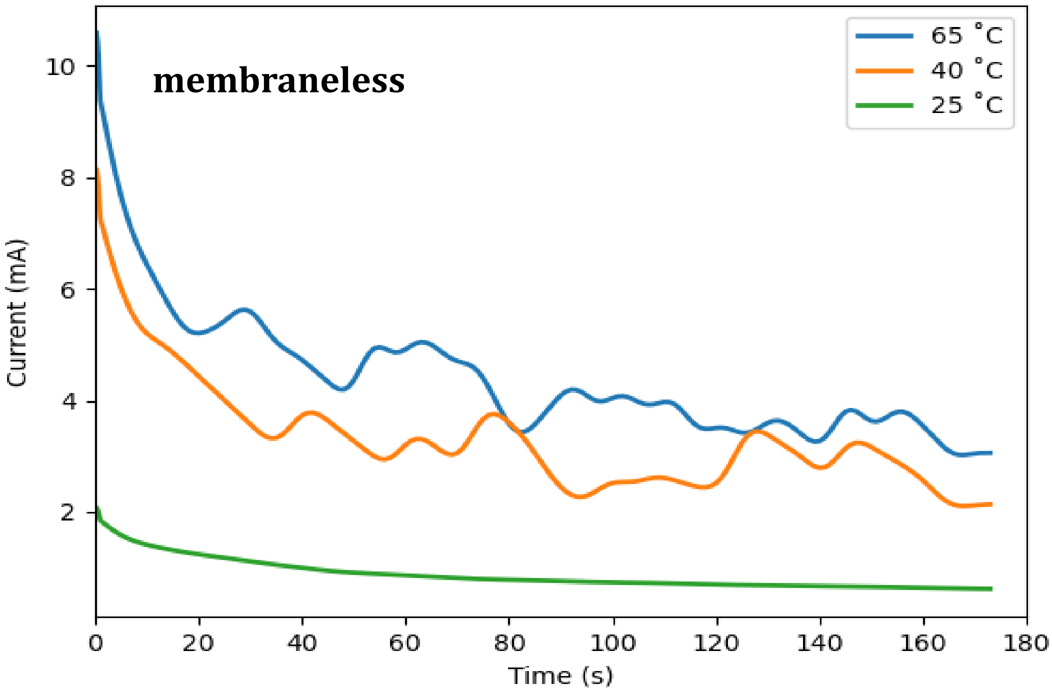

Figure 5.6 The effect of temperature on the hydrogen production at the flow rates of 5 ml/min at the potential of 2.0 V in the electrolyte of 2 M KOH solution.

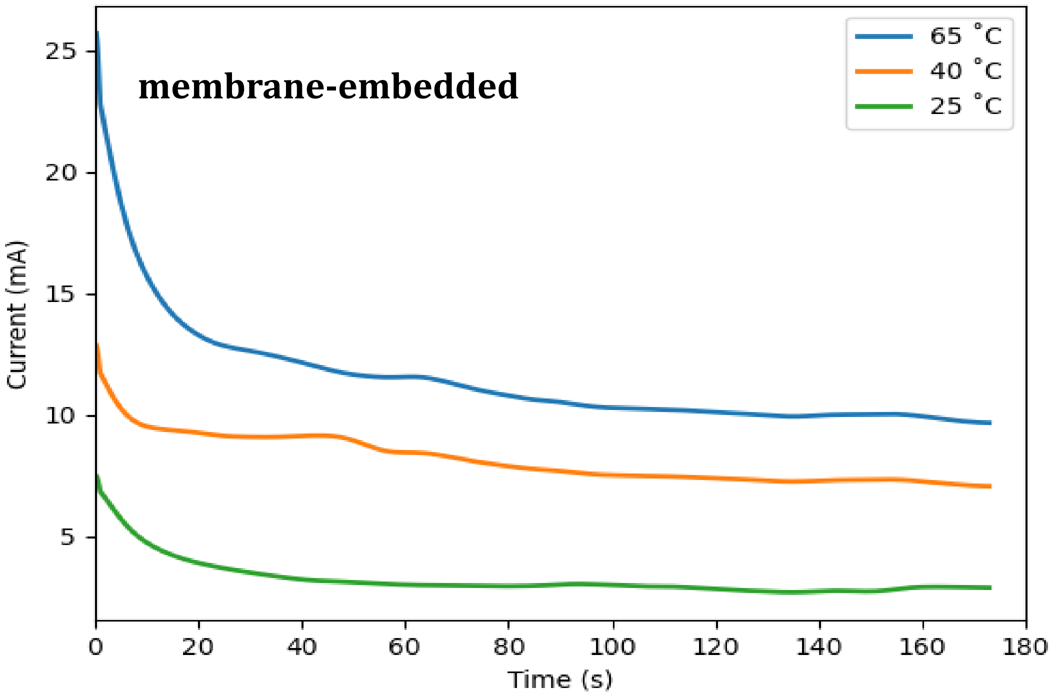

Figure 5.7 The effect of temperature on the hydrogen production at the flow rates of 5 ml/min at the potential of 2.0 V in the electrolyte of 2 M KOH solution.

5.3.2.3 Applied Potential

We conducted experiments at three different fixed applied voltages to assess its effects coordinated with temperature and flow rate on gas bubble removal. It was important to be able to apply constant voltage during electrolysis in order to achieve more efficient systems. When steady DC is applied, net efficiency may be achieved between 56-73% [79]. In case steady DC is achieved, it is relatively easy to interpret that the higher fixed cell potentials yield the higher amounts of hydrogen gas. However, the more hydrogen produced; the more resistance observed to the electrochemical reaction. Nevertheless, the values of the recorded currents folded in the membrane-embedded electrolyzer comparing to the membraneless one at higher cell voltages. These results supported the idea that our membrane-embedded electrolyzer significantly removed gas bubbles from its pores; hence, more efficient systems can be obtained directly proportionally to voltage.

Tables 5.3 and 5.4 compare the total amount of hydrogen produced for different cell potentials with respect to cell potential of 1.8 V at the temperatures of 25 ˚C, 40 ˚C, and 65 ˚C and the flow rates of 5 ml/min in the membrane-embedded and membraneless electrolyzers, respectively. The calculations show that the total amount of hydrogen production increased with the increasing cell voltages, in good agreement with the literature. Moreover, hydrogen production was increased incrementally when constant cell potential hit the 2.2 V in the membrane-embedded electrolyzer. These significant increases of hydrogen production; however, were not as high as for the membraneless electrolyzer operating at the same conditions (2.2 V and 5 ml/min). This comparison was proof regarding the hydrophobic membrane we selected would be an efficient solution for the bubble-related challenges under the conditions of a high gas bubble accumulation (at high voltages or temperatures). Likewise, we compared the same in Tables 5.5 and 5.6 based on the measurements of 1 ml/min operating flow rates for membrane-embedded and membraneless electrolyzers, respectively. The maximum value was obtained as 25 in the membrane-embedded electrolyzer operating at the lower flow rate and temperature and higher cell voltage (1 ml/min, 25 ˚C and 2.2 V for our experimental conditions). These results affirmed our former interpretation regarding whether the membrane was working. Moreover, our membrane-embedded design can be easily integrated into thermal or waste heat sources, such as PV, requiring more contact time of the electrolyte with the electrodes (lower flow rates).

Table 5.3 The ratio of total hydrogen production at various cell potentials to those at the 1.8 V operating voltage at the temperatures of 25 ˚C, 40 ˚C, and 65 ˚C (based on the results of the membrane-embedded electrolyzers operating at 5 ml/min flow rate).

Cell Potential (V)	The ratio wrt 1.8 V @ 25 ˚C	The ratio wrt 1.8 V @ 40 ˚C	The ratio wrt 1.8 V @ 65 ˚C
1.8	1	1	1
2.0	2.33	5.10	4.88
2.2	9.23	10.84	9.96

Table 5.4 The ratio of total hydrogen production at various cell potentials to those at the 1.8 V operating voltage at the temperatures of 25 ˚C, 40 ˚C, and 65 ˚C (based on the results of the membraneless electrolyzers operating at 5 ml/min flow rate).

Cell Potential (V)	The ratio wrt 1.8 V @ 25 ˚C	The ratio wrt 1.8 V @ 40 ˚C	The ratio wrt 1.8 V @ 65 ˚C
1.8	1	1	1
2.0	1.55	4.66	4.77
2.2	2.00	5.62	6.34

Table 5.5 The ratio of total hydrogen production at various cell potentials to those at the 1.8 V operating voltage at the temperatures of 25 ˚C, 40 ˚C, and 65 ˚C (based on the results of the membrane-embedded electrolyzers operating at 1 ml/min flow rate).

Cell Potential (V)	The ratio wrt 1.8 V @ 25 ˚C	The ratio wrt 1.8 V @ 40 ˚C	The ratio wrt 1.8 V @ 65 ˚C
1.8	1	1	1
2.0	6.49	4.37	5.16
2.2	25.01	11.63	11.95

Table 5.6 The ratio of total hydrogen production at various cell potentials to those at the 1.8 V operating voltage at the temperatures of 25 ˚C, 40 ˚C, and 65 ˚C (based on the results of the membraneless electrolyzers operating at 1 ml/min flow rate).

Cell Potential (V)	The ratio wrt 1.8 V @ 25 ˚C	The ratio wrt 1.8 V @ 40 ˚C	The ratio wrt 1.8 V @ 65 ˚C
1.8	1	1	1
2.0	1.43	1.78	1.35
2.2	2.91	1.71	1.46

5.4 Constant Current Measurements and Overall Electrolysis Efficiency

Theoretically, the minimum required voltage (reversible voltage) to initiate the water electrolysis reaction is 1.23 V at standard temperature and pressure. However, the cell voltage is higher in commercial electrolyzers because of the activation, ohmic, and concentration overpotentials [80]. Commercially, alkaline water electrolyzers operate mostly at 1.8-2.0 V [10]. Different studies have been conducted to decrease overpotentials, such as using different types of materials or treatments and arranging operating parameters [32]. Gas bubble formation in electrolytic systems is a challenging overpotential reason, especially when dimensions are reduced to microfluidic levels, leading to higher power consumption [57]. A planar structure with flowing streams of the electrolyte would be beneficial to remove bubbles; however, this type of electrolyzers tend to achieve lower efficiencies. Therefore, we analyzed bubble overvoltage in our constant current experiments by comparing operating voltages of membraneless and gas bubble-reduced membrane-embedded electrolyzers.

Voltages were recorded by keeping constant current densities as 0.6 mA/cm^2 and 1.7 mA/cm^2 during the electrolysis for the membrane-embedded and membraneless microfluidic electrolyzers. Under similar conditions, performance improvements (lower voltages measurements) of the membraneless electrolyzers with the embedment of the membranes would give evidence of whether the selected membrane was working. In Figure 5.8.a and 5.8.b, corresponding experimental voltages as a function of time at the flow rate of 5 ml/min and the temperature of 40 ˚C can be seen. Based on the figures, we obtained more stable graphs and lower voltages from the membrane-embedded electrolyzers for both 0.6 mA/cm^2 and 1.7 mA/cm^2. Obtained low and stable graph patterns prove the predictions regarding membrane-embedded electrolyzer design supplied rapid gas bubble removal.

Numerically, comparing the energetic efficiencies was necessary to understand if bubble overpotential decreased with the help of membrane embedment. Figure 5.9 indicates the calculated overall electrolysis efficiencies as a function of temperature for the membrane-embedded and membraneless electrolyzers at the operating flow rates of 5 ml/min and 1 ml/min. As expected, the maximum efficiency was achieved in the membrane-embedded electrolyzer at the flow rate of 5 ml/min and the temperature of 65 ˚C with a value of 0.72. Because, higher flow rates, as well as the porous membrane, supported the removal of gas bubbles from the microchannel. While the only difference was the removal of the membrane, the overall electrolysis efficiency decreased to the value of 0.67. In this situation, the flow rate was the only effect on bubble removal; therefore, we observed the efficiency decrease. When the flow rate was also decreased to 1 ml/min; however, the lowest overall electrolysis efficiency was obtained as the value of 0.52 in the membraneless electrolyzer. Gas bubbles formed densely because of high temperature and applied voltage; then, stuck in microchannels. Therefore, the removal of them was performed with neither factor of porous membrane nor flow rate. However, no decline was observed in the membrane-embedded electrolyzer even at the flow rate of 1 ml/min, proving our hypothesis regarding the porous hydrophobic membrane allows rapid gas bubble removal. Although higher efficiencies can be obtained by using the membrane at the relatively higher operating flow rates, it was possible to use a membrane-embedded electrolyzer for systems that require lower operating flow rates, requiring more residence time to benefit from thermal sources during electrolysis [2] since this design also solved the clogging problems at lower operating flow rates.

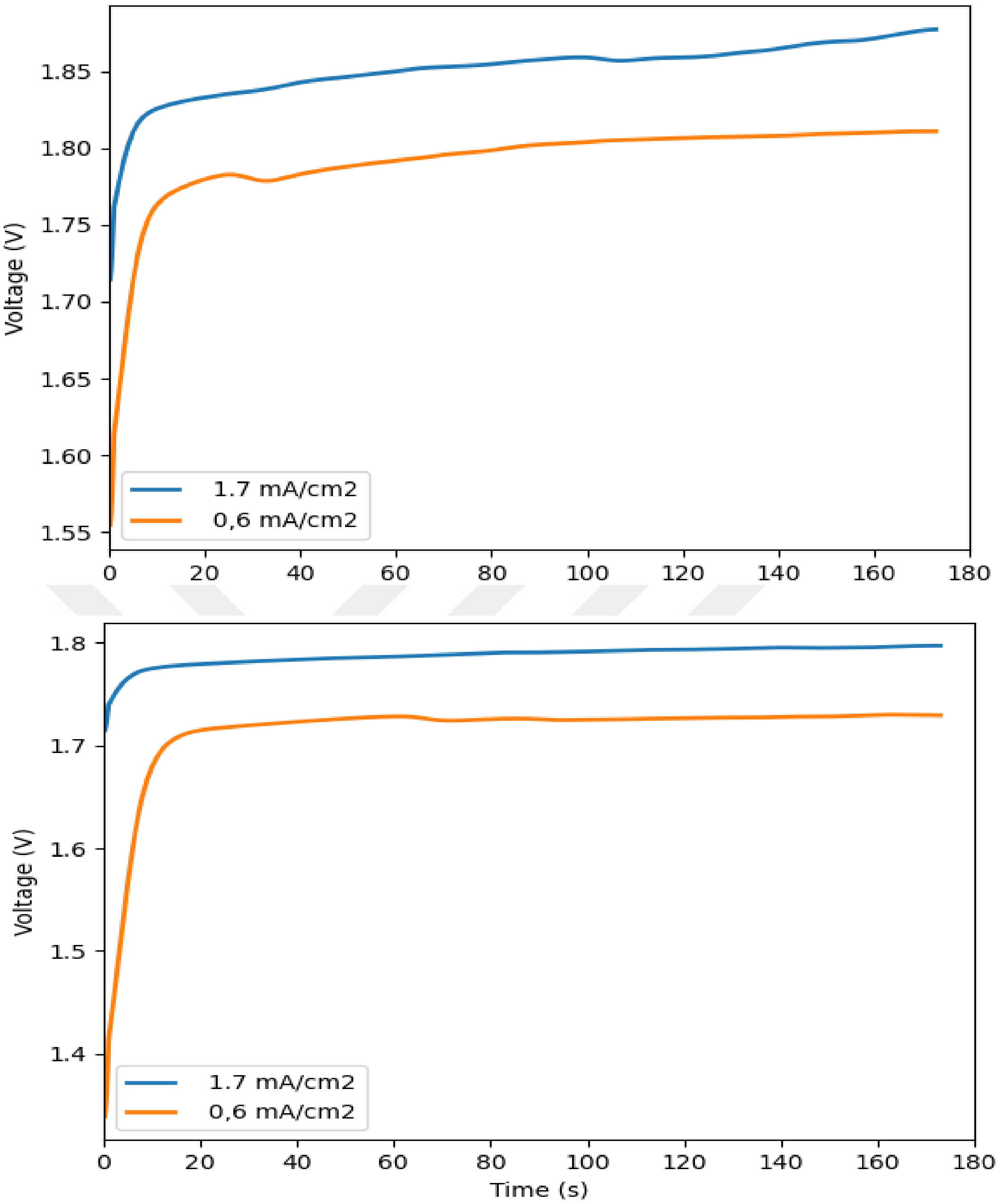

Figure 5.8 The hydrogen production voltages at the flow rate of 5 ml/ min at the temperature of 40 ˚C, and the constant currents of 0.6 mA and 1.7 mA with the 2 M KOH electrolyte solution a) membraneless electrolyzer b) membrane-assembled electrolyzer.

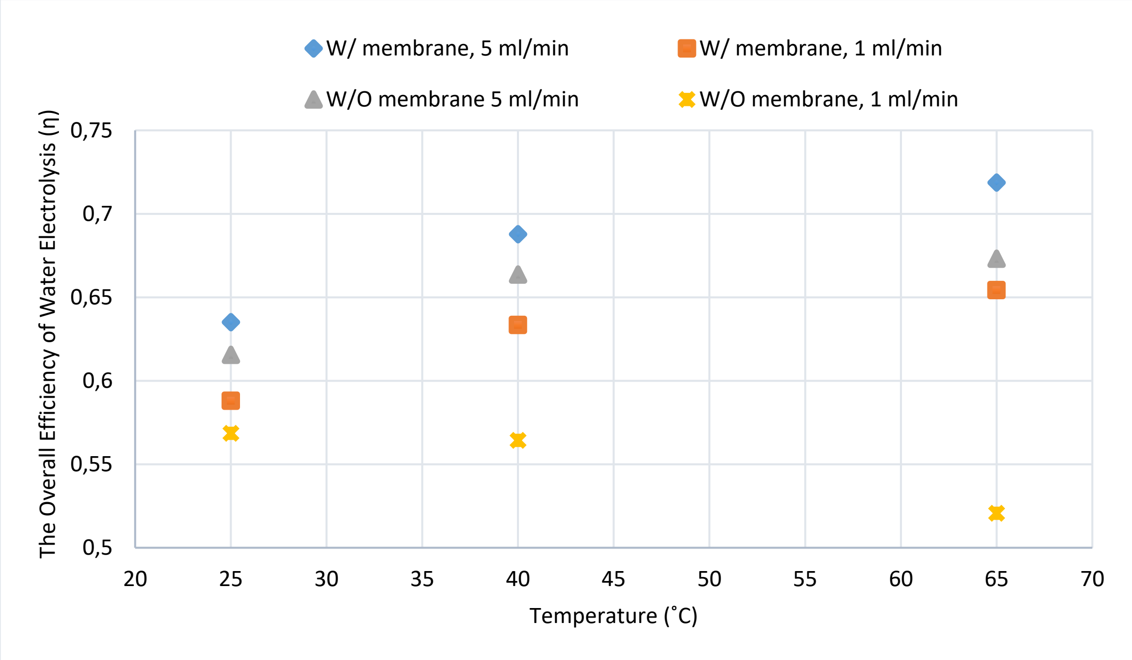

Figure 5.9 The overall efficiency of water electrolysis in the membrane-assembled and membraneless electrolyzers at the temperatures of 25 ˚C, 40 ˚C, 65 ˚C and at the flow rates of 5 ml/min and 1 ml/min.

5.5 Conclusion & Future Perspectives

This present proof-of-concept study has described the design stages of planar alkaline microfluidic water electrolyzers with and without polytetrafluoroethylene (PTFE) hydrophobic membrane to produce hydrogen more efficiently. We achieved the same experimental conditions regarding materials selection and assembling steps of electrolyzers, and operating parameters, such as temperature, flow rate, and applied voltage for both electrolyzers. By utilizing a PTFE membrane, the gas bubbles were removed proportionately; so that, the negative impacts of two-phase flow were diminished and blockage of the microchannel was mitigated. The highest energetic efficiency was calculated at optimum electrolyzer design, which was PTFE hydrophobic membrane integrated, and at optimum operating parameters, which was 65 ˚C temperature and 5 ml/min flow rate.

In accordance with our purposes, the following conclusions were achieved

- No leakage was observed up to the water entry pressure of the membrane.

- The membrane we used was appropriate to pass gases through its pores, and the blockage of the microchannel was mitigated.
- The efficiency of the membrane-embedded electrolyzer was achieved as 0.72 at 65 ˚C and 5 ml/min.
- The amount of hydrogen production increased with the increase in temperature, flow rate and applied voltage, in good agreement with the literature.

These results are summarized by comparing the amounts of hydrogen produced from the electrolyzers operating at various temperatures, flow rates and applied voltages, which were indicated in the following tables.

Table 5.7 The amount of hydrogen produced from the electrolyzers operating at various temperatures and applied voltages, and the flow rate of 5 ml/min. (Calculations were done based on the data after reaching steady-state behavior.)

Electrolyzer	**Cell Potential**	**The amount of hydrogen ($ml.h^{-1}.cm^{-2}$)**		
		@ 25 ˚C	**@ 40 ˚C**	**@ 65 ˚C**
Membrane-embedded	1.8	0.60	0.76	1.31
	2.0	1.44	3.95	5.84
	2.2	5.79	8.87	11.48
Membraneless	1.8	0.27	0.34	0.50
	2.0	0.36	1.47	2.13
	2.2	0.47	1.97	2.76

Table 5.8 The amount of hydrogen produced from the electrolyzers operating at various temperatures and applied voltages, and the flow rate of 1 ml/min. (Calculations were done based on the data after reaching steady-state behavior.)

Electrolyzer	Cell Potential	The amount of hydrogen ($ml.h^{-1}.cm^{-2}$)		
		@ 25 ˚C	@ 40 ˚C	@ 65 ˚C
Membrane-embedded	1.8	0.17	0.55	0.61
	2.0	1.20	2.12	2.84
	2.2	4.22	5.68	6.88
Membraneless	1.8	0.14	0.25	0.37
	2.0	0.20	0.38	0.56
	2.2	0.34	0.38	0.58

As future work, a waste heat recovery model can be developed by integrating our membrane-embedded electrolyzer design into a waste heat source to reduce energy consumption while keeping high efficiencies of the electrolyzer. For instance, photovoltaic technologies convert solar energy into electricity. However, dissipated heat that is not converted into electricity leads to decreasing in photovoltaic module efficiency while operating. Therefore, this dissipated heat can be used to elevate the electrolyte temperature rather than utilizing electrical energy for the heating electrolyte. This integrated-model would also be advantageous to reduce the energy consumption of photovoltaic cooling systems. In such an integrated-system, lower flow rates may be preferred to allow more time to contact between the electrolyte and the waste heat source. Therefore, as our membrane-integrated electrolyzer is also efficient at the lower flow rate (which was 1 ml/min in the present work), it would be appropriate to utilize it in such a hybrid system. Accordingly, the optimum electrolyte temperature for an efficient electrolyzer will be determined, and to absorb the required heat from the waste heat source, the necessary flow rate will be estimated. Moreover, a membrane having different properties such as pore diameter, porosity, or hydrophobicity as well as various types of them can be utilized to compare the current system and achieve better efficiencies.

REFERENCES

[1] A. M. Abdalla, S. Hossain, O. B. Nisfindy, A. T. Azad, M. Dawood, and A. K. Azad, "Hydrogen production, storage, transportation and key challenges with applications: A review," (in English), *Energy Conversion and Management,* Review vol. 165, pp. 602-627, Jun 2018.

[2] D. D. D. Palhares, L. G. M. Vieira, and J. J. R. Damasceno, "Hydrogen production by a low-cost electrolyzer developed through the combination of alkaline water electrolysis and solar energy use," (in English), *International Journal of Hydrogen Energy,* Article vol. 43, no. 9, pp. 4265-4275, Mar 2018.

[3] A. Ursua, I. S. Martin, E. L. Barrios, and P. Sanchis, "Stand-alone operation of an alkaline water electrolyser fed by wind and photovoltaic systems," (in English), *International Journal of Hydrogen Energy,* Article vol. 38, no. 35, pp. 14952-14967, Nov 2013.

[4] A. A. AlZahrani and I. Dincer, "Thermodynamic and electrochemical analyses of a solid oxide electrolyzer for hydrogen production," (in English), *International Journal of Hydrogen Energy,* Article; Proceedings Paper vol. 42, no. 33, pp. 21404-21413, Aug 2017.

[5] M. Y. Lin, L. W. Hourng, S. H. Huang, T. H. Tsai, and W. N. Hsu, "Analysis and Study on Polarization during Water Electrolysis Hydrogen Production," (in English), *Chemical Engineering Communications,* Article vol. 204, no. 2, pp. 168-175, 2017.

[6] A. Ursua, L. M. Gandia, and P. Sanchis, "Hydrogen Production From Water Electrolysis: Current Status and Future Trends (vol 100, pg 410, 2012)," (in English), *Proceedings of the Ieee,* Correction vol. 100, no. 3, pp. 811-811, Mar 2012.

[7] L. Jiang, B. Myer, K. Tellefsen, and S. Pau, "A planar microfabricated electrolyzer for hydrogen and oxygen generation," (in English), *Journal of Power Sources,* Article vol. 188, no. 1, pp. 256-260, Mar 2009.

[8] H. Ishaq and I. Dincer, "Comparative assessment of renewable energy-based hydrogen production methods," (in English), *Renewable & Sustainable Energy Reviews,* Article vol. 135, p. 13, Jan 2021, Art. no. 110192.

[9] P. Nikolaidis and A. Poullikkas, "A comparative overview of hydrogen production processes," (in English), *Renewable & Sustainable Energy Reviews,* Review vol. 67, pp. 597-611, Jan 2017.

[10] I. Dincer and C. Acar, "Review and evaluation of hydrogen production methods for better sustainability," (in English), *International Journal of Hydrogen Energy,* Review vol. 40, no. 34, pp. 11094-11111, Sep 2015.

[11] M. E. Oruc, A. V. Desai, P. J. A. Kenis, and R. G. Nuzzo, "Comprehensive energy analysis of a photovoltaic thermal water electrolyzer," (in English), *Applied Energy,* Article vol. 164, pp. 294-302, Feb 2016.

[12] T. L. Gibson and N. A. Kelly, "Optimization of solar powered hydrogen production using photovoltaic electrolysis devices," (in English), *International Journal of Hydrogen Energy,* Article vol. 33, no. 21, pp. 5931-5940, Nov 2008.

[13] J. R. Bartels, M. B. Pate, and N. K. Olson, "An economic survey of hydrogen production from conventional and alternative energy sources," (in English), *International Journal of Hydrogen Energy,* Article vol. 35, no. 16, pp. 8371-8384, Aug 2010.

[14] P.-l.-O. Pierre Jonville, "Electrolyzer with Released Gas," Apr. 25, 1978.

[15] H. Cho, J. Kim, and K. H. Han, "An assembly disposable degassing microfluidic device using a gas-permeable hydrophobic membrane and a reusable microsupport array," (in English), *Sensors and Actuators B-Chemical,* Article vol. 286, pp. 353-361, May 2019.

[16] C. C. Liu, J. A. Thompson, and H. H. Bau, "A membrane-based, high-efficiency, microfluidic debubbler," (in English), *Lab on a Chip,* Article vol. 11, no. 9, pp. 1688-1693, 2011.

[17] J. Xu, R. Vaillant, and D. Attinger, "Use of a porous membrane for gas bubble removal in microfluidic channels: physical mechanisms and design criteria," (in English), *Microfluidics and Nanofluidics,* Article vol. 9, no. 4-5, pp. 765-772, Oct 2010.

[18] N. Nagai, M. Takeuchi, T. Kimura, and T. Oka, "Existence of optimum space between electrodes on hydrogen production by water electrolysis," (in English), *International Journal of Hydrogen Energy,* Article vol. 28, no. 1, pp. 35-41, Jan 2003, Art. no. Pii s0360-3199(02)00027-7.

[19] N. Nagai, M. Takeuchi, and M. Nakao, "Effects of generated bubbles between electrodes on efficiency of alkaline water electrolysis," (in English), *Jsme International Journal Series B-Fluids and Thermal Engineering,* Article; Proceedings Paper vol. 46, no. 4, pp. 549-556, Nov 2003.

[20] O. Winther-Jensen, K. Chatjaroenporn, B. Winther-Jensen, and D. R. MacFarlane, "Towards hydrogen production using a breathable electrode structure to directly separate gases in the water splitting reaction," (in English), *International Journal of Hydrogen Energy,* Article vol. 37, no. 10, pp. 8185-8189, May 2012.

[21] T. Vilasmongkolchai, R. Songprakorp, and K. Sudaprasert, "The Behaviour of Gas Bubble during Rest Period of Pulse-Activated Electrolysis Hydrogen Production," in *2016 3rd International Conference on Mechanics and Mechatronics Research*, vol. 77, D. Zhang, B. Zi, G. Cui, and H. Ding, Eds. (MATEC Web of Conferences, Cedex A: E D P Sciences, 2016.

[22] H. G. Derami, R. Vundavilli, and J. Darabi, "Experimental and computational study of gas bubble removal in a microfluidic system using nanofibrous membranes," (in English), *Microsystem Technologies-Micro-and Nanosystems-Information Storage and Processing Systems,* Article vol. 23, no. 7, pp. 2685-2698, Jul 2017.

[23] P. Tiwari, G. Tselzouras, K. Wagner, G. F. Swiegers, and G. G. Wallace, "A new class of bubble-free water electrolyzer that is intrinsically highly efficient," (in English), *International Journal of Hydrogen Energy,* Article vol. 44, no. 42, pp. 23568-23579, Sep 2019.

[24] M. E. Oruc, A. V. Desai, R. G. Nuzzo, and P. J. A. Kenis, "Design, fabrication, and characterization of a proposed microchannel water electrolyzer," (in English), *Journal of Power Sources,* Article vol. 307, pp. 122-128, Mar 2016.

[25] S. Z. Baykara, "Hydrogen: A brief overview on its sources, production and environmental impact," (in English), *International Journal of Hydrogen Energy,* Article vol. 43, no. 23, pp. 10605-10614, Jun 2018.

[26] B. Coelho, A. C. Oliveira, and A. Mendes, "Concentrated solar power for renewable electricity and hydrogen production from water-a review," (in English), *Energy & Environmental Science,* Article vol. 3, no. 10, pp. 1398-1405, 2010.

[27] H. B. Liu, L. M. Pan, Q. J. Qin, and P. F. Li, "Experimental and numerical investigation of gas-liquid flow in water electrolysis under magnetic field," (in English), *Journal of Electroanalytical Chemistry,* Article vol. 832, pp. 293-302, Jan 2019.

[28] E. Commission. (July, 2020). *A Hydrogen Strategy for a climate neutral Europe*. Available: https://ec.europa.eu/energy/topics/energy-system-integration/hydrogen_en

[29] K. C. Sandeep *et al.*, "Experimental studies and modeling of advanced alkaline water electrolyser with porous nickel electrodes for hydrogen production," (in English), *International Journal of Hydrogen Energy,* Article vol. 42, no. 17, pp. 12094-12103, Apr 2017.

[30] P. M. Dieguez, A. Ursua, P. Sanchis, C. Sopena, E. Guelbenzu, and L. M. Gandia, "Thermal performance of a commercial alkaline water electrolyzer: Experimental study and mathematical modeling," (in English), *International Journal of Hydrogen Energy,* Article vol. 33, no. 24, pp. 7338-7354, Dec 2008.

[31] M. Carmo, D. L. Fritz, J. Merge, and D. Stolten, "A comprehensive review on PEM water electrolysis," (in English), *International Journal of Hydrogen Energy,* Review vol. 38, no. 12, pp. 4901-4934, Apr 2013.

[32] Z. Abdin, C. J. Webb, and E. M. Gray, "Modelling and simulation of an alkaline electrolyser cell," (in English), *Energy,* Article vol. 138, pp. 316-331, Nov 2017.

[33] O. Ulleberg, "Modeling of advanced alkaline electrolyzers: a system simulation approach," (in English), *International Journal of Hydrogen Energy,* Article vol. 28, no. 1, pp. 21-33, Jan 2003, Art. no. Pii s0360-3199(02)00033-2.

[34] A. Ursua, L. Marroyo, E. Gubia, L. M. Gandia, P. M. Dieguez, and P. Sanchis, "Influence of the power supply on the energy efficiency of an alkaline water electrolyser," (in English), *International Journal of Hydrogen Energy,* Article vol. 34, no. 8, pp. 3221-3233, May 2009.

[35] K. Onda, T. Kyakuno, K. Hattori, and K. Ito, "Prediction of production power for high-pressure hydrogen by high-pressure water electrolysis," (in English), *Journal of Power Sources,* Article vol. 132, no. 1-2, pp. 64-70, May 2004.

[36] R. W. Guo, T. T. Fu, C. Y. Zhu, and Y. G. Ma, "Pressure drop model of gas-liquid flow with mass transfer in tree-typed microchannels," (in English), *Chemical Engineering Journal,* Article vol. 397, p. 11, Oct 2020, Art. no. 125340.

[37] L. E. O'Neill and I. Mudawar, "Review of two-phase flow instabilities in macro- and micro-channel systems," (in English), *International Journal of Heat and Mass Transfer,* Review vol. 157, p. 43, Aug 2020, Art. no. 119738.

[38] A. Hibara *et al.*, "Surface modification method of microchannels for gas-liquid two-phase flow in microchips," (in English), *Analytical Chemistry,* Article vol. 77, no. 3, pp. 943-947, Feb 2005.

[39] M. P. David, J. Miler, J. E. Steinbrenner, Y. Z. Yang, M. Touzelbaev, and K. E. Goodson, "Hydraulic and thermal characteristics of a vapor venting two-phase microchannel heat exchanger," (in English), *International Journal of Heat and Mass Transfer,* Article vol. 54, no. 25-26, pp. 5504-5516, Dec 2011.

[40] R. S. Abiev, "Analysis of local pressure gradient inversion and form of bubbles in Taylor flow in microchannels," (in English), *Chemical Engineering Science,* Article vol. 174, pp. 403-412, Dec 2017.

[41] M. Pietrzak and M. Placzek, "Void fraction predictive methods in two-phase flow across a small diameter channel," (in English), *International Journal of Multiphase Flow,* Review vol. 121, p. 7, Dec 2019, Art. no. 103115.

[42] K. De Kerpel, B. Ameel, C. T'Joen, H. Caniere, and M. De Paepe, "Flow regime based calibration of a capacitive void fraction sensor for small diameter tubes," (in English), *International Journal of Refrigeration-Revue Internationale Du Froid,* Article vol. 36, no. 2, pp. 390-401, Mar 2013.

[43] E. X. Barreto, J. L. G. Oliveira, and J. C. Passos, "Frictional pressure drop and void fraction analysis in air-water two-phase flow in a microchannel," (in English), *International Journal of Multiphase Flow,* Article vol. 72, pp. 1-10, Jun 2015.

[44] A. E. H. a. M. L. STANLEY M. BARNETT, "Bubble Motion and Mass Transfer in Non-Newtonian Fluids," *A.1.Ch.E. Journal,* vol. 12, pp. 253-259, March 1966.

[45] Y. Y. Bao, Z. C. Jiang, S. F. Tong, X. B. Huang, Z. Q. Cai, and Z. M. Gao, "Reactive mass transfer of single O-2 bubbles in a turbulent flow chamber," (in English), *Chemical Engineering Science,* Article vol. 207, pp. 829-843, Nov 2019.

[46] R. A. Shellie, H. J. Cortes, R. Gras, and J. Luong, "Planar microfluidic devices in flow modulated comprehensive two dimensional gas chromatography for challenging petrochemical applications," (in English), *Analytical Methods,* Article vol. 5, no. 23, pp. 6598-6604, 2013.

[47] Y. N. He and T. Leichle, "Fabrication of lateral porous silicon membranes for planar microfluidics by means of ion implantation," (in English), *Sensors and Actuators B-Chemical,* Article vol. 239, pp. 628-634, Feb 2017.

[48] F. Dubosc, D. Bourrier, and T. Leichle, "Fabrication of lateral porous silicon membranes for planar microfluidic devices," in *26th European Conference on Solid-State Transducers, Eurosensor 2012*, vol. 47, R. Walczak and J. Dziuban, Eds. (Procedia Engineering, Amsterdam: Elsevier Science Bv, 2012, pp. 801-804.

[49] J. R. Hoffman and W. A. Phillip, "100th Anniversary of Macromolecular Science Viewpoint: Integrated Membrane Systems," (in English), *Acs Macro Letters,* Article vol. 9, no. 9, pp. 1267-1279, Sep 2020.

[50] J. Hereijgers, G. Desmet, T. Breugelmans, and W. De Malsche, "Strategies to integrate porous layers in microfluidic devices," (in English), *Microelectronic Engineering,* Review vol. 132, pp. 1-13, Jan 2015.

[51] S. G. v. I. K. Vedat Uyak, *Su/Atıksu Arıtılması ve Geri Kazanılmasında Membran Teknolojileri ve Uygulamaları*. 2018.

[52] J. Zhao *et al.*, "Tailoring waterproof and breathable properties of environmentally friendly electrospun fibrous membranes by optimizing porous structure and surface wettability," (in English), *Composites Communications,* Article vol. 15, pp. 40-45, Oct 2019.

[53] V. Boffa, L. Parmeggiani, A. H. Nielsen, and G. Magnacca, "Hydrophilicity and surface heterogeneity of TiO2-doped silica materials for membrane applications," (in English), *Microporous and Mesoporous Materials,* Article vol. 221, pp. 81-90, Feb 2016.

[54] S. Mosadegh-Sedghi, D. Rodrigue, J. Brisson, and M. C. Iliuta, "Wetting phenomenon in membrane contactors - Causes and prevention," (in English), *Journal of Membrane Science,* Review vol. 452, pp. 332-353, Feb 2014.

[55] J. G. Lu, Y. F. Zheng, and M. D. Cheng, "Wetting mechanism in mass transfer process of hydrophobic membrane gas absorption," (in English), *Journal of Membrane Science,* Article vol. 308, no. 1-2, pp. 180-190, Feb 2008.

[56] P. S. Goh, R. Naim, M. Rahbari-Sisakht, and A. F. Ismail, "Modification of membrane hydrophobicity in membrane contactors for environmental remediation," (in English), *Separation and Purification Technology,* Review vol. 227, p. 19, Nov 2019, Art. no. 115721.

[57] D. D. Meng, T. Cubaud, C. M. Ho, and C. J. Kim, "A methanol-tolerant gas-venting microchannel for a microdirect methanol fuel cell," (in English), *Journal of Microelectromechanical Systems,* Article vol. 16, no. 6, pp. 1403-1410, Dec 2007.

[58] V. Y. Dindore, D. W. F. Brilman, F. H. Geuzebroek, and G. F. Versteeg, "Membrane-solvent selection for CO2 removal using membrane gas-liquid contactors," (in English), *Separation and Purification Technology,* Article vol. 40, no. 2, pp. 133-145, Dec 2004.

[59] J. V. Dobson and M. J. Taylor, "ELECTROCHEMICALLY DERIVED VALUES OF THE PERMEABILITY COEFFICIENT OF COMMON GASES THROUGH PTFE MEMBRANES BETWEEN 9 AND 41-DEGREES-C," (in English), *Electrochimica Acta,* Article vol. 31, no. 2, pp. 235-239, Feb 1986.

[60] M. S. Ismail *et al.*, "Through-Plane Permeability for Untreated and PTFE-Treated Gas Diffusion Layers in Proton Exchange Membrane Fuel Cells," (in English), *Journal of Fuel Cell Science and Technology,* Article vol. 7, no. 5, p. 7, Oct 2010, Art. no. 051016.

[61] H. Kim, T. Yun, S. Hong, and S. Lee, "Experimental and theoretical investigation of a high performance PTFE membrane for vacuum-membrane distillation," (in English), *Journal of Membrane Science,* Article vol. 617, p. 6, Jan 2021, Art. no. 118524.

[62] J. V. Dobson and M. J. Taylor, "THE PERMEABILITY OF GASES THROUGH PTFE AND OTHER MEMBRANES AT 25-DEGREES-C," (in English), *Electrochimica Acta,* Article vol. 31, no. 2, pp. 231-233, Feb 1986.

[63] R. Vundavilli, J. Darabi, and Asme, *Bubble Removal in Microfluidic Devices Using Nanofibrous Membranes* (Proceedings of the Asme 12th International Conference on Nanochannels, Microchannels, and Minichannels, 2014). New York: Amer Soc Mechanical Engineers, 2014.

[64] D. T. Eddington, "In-line microfluidic bubble trap," F. Burgoyne, Ed., ed. Royal Society of Chemistry, 2006.

[65] A. M. Skelley and J. Voldman, "An active bubble trap and debubbler for microfluidic systems," (in English), *Lab on a Chip,* Article vol. 8, no. 10, pp. 1733-1737, Oct 2008.

[66] B. H. Timmer, K. M. van Delft, W. Olthuis, P. Bergveld, and A. van den Berg, "Micro-evaporation electrolyte concentrator," (in English), *Sensors and Actuators B-Chemical,* Article; Proceedings Paper vol. 91, no. 1-3, pp. 342-346, Jun 2003.

[67] X. F. He, R. Chen, X. Zhu, Q. Liao, and S. Z. Li, "Laser assisted microfluidic membrane evaporator for sample crystallization separation," (in English), *Separation and Purification Technology,* Article vol. 242, p. 8, Jul 2020, Art. no. 116817.

[68] M. Qasim, D. D. Duong, J. Y. Lee, and N. Y. Lee, "Fabrication of polycaprolactone nanofibrous membrane-embedded microfluidic device for water filtration," (in English), *Journal of Applied Polymer Science,* Article vol. 137, no. 40, p. 10, Oct 2020, Art. no. e49207.

[69] R. H. Petrucci and W. S. Harwood, P. F. Corey, Ed. *General Chemistry: Principles and Modern Applications*, 7th Edition ed. Upper Saddle River, New Jersey 07458: Prentice-Hall International, Inc., 1997.

[70] A. Gunther, M. Jhunjhunwala, M. Thalmann, M. A. Schmidt, and K. F. Jensen, "Micromixing of miscible liquids in segmented gas-liquid flow," (in English), *Langmuir,* Article vol. 21, no. 4, pp. 1547-1555, Feb 2005.

[71] A. Gunther, S. A. Khan, M. Thalmann, F. Trachsel, and K. F. Jensen, "Transport and reaction in microscale segmented gas-liquid flow," (in English), *Lab on a Chip,* Article vol. 4, no. 4, pp. 278-286, 2004.

[72] D. L. Stojic, M. P. Marceta, S. P. Sovilj, and S. S. Miljanic, "Hydrogen generation from water electrolysis - possibilities of energy saving," (in English), *Journal of Power Sources,* Article; Proceedings Paper vol. 118, no. 1-2, pp. 315-319, May 2003.

[73] M. H. Sellami and K. Loudiyi, "Electrolytes behavior during hydrogen production by solar energy," (in English), *Renewable & Sustainable Energy Reviews,* Review vol. 70, pp. 1331-1335, Apr 2017.

[74] C. Lupi, A. Dell'Era, and M. Pasquali, "Nickel-cobalt electrodeposited alloys for hydrogen evolution in alkaline media," (in English), *International Journal of Hydrogen Energy,* Article vol. 34, no. 5, pp. 2101-2106, Mar 2009.

[75] J. H. Sung and M. L. Shuler, "Prevention of air bubble formation in a microfluidic perfusion cell culture system using a microscale bubble trap," (in English), *Biomedical Microdevices,* Article vol. 11, no. 4, pp. 731-738, Aug 2009.

[76] J. Eigeldinger and H. Vogt, "The bubble coverage of gas-evolving electrodes in a flowing electrolyte," (in English), *Electrochimica Acta,* Article vol. 45, no. 27, pp. 4449-4456, 2000.

[77] H. Vogt and R. J. Balzer, "The bubble coverage of gas-evolving electrodes in stagnant electrolytes," (in English), *Electrochimica Acta,* Review vol. 50, no. 10, pp. 2073-2079, Mar 2005.

[78] M. Schalenbach, G. Tjarks, M. Carmo, W. Lueke, M. Mueller, and D. Stolten, "Acidic or Alkaline? Towards a New Perspective on the Efficiency of Water Electrolysis," (in English), *Journal of the Electrochemical Society,* Article vol. 163, no. 11, pp. F3197-F3208, 2016.

[79] Z. Dobo and A. B. Palotas, "Impact of the voltage fluctuation of the power supply on the efficiency of alkaline water electrolysis," (in English), *International Journal of Hydrogen Energy,* Article vol. 41, no. 28, pp. 11849-11856, Jul 2016.

[80] E. Amores, J. Rodriguez, and C. Carreras, "Influence of operation parameters in the modeling of alkaline water electrolyzers for hydrogen production," (in English), *International Journal of Hydrogen Energy,* Article vol. 39, no. 25, pp. 13063-13078, Aug 2014.

PUBLICATIONS FROM THE THESIS

Contact Information: nurdanmese@gmail.com

Conference Papers

1. N. Mese, H. Sadikoglu, M.E. Oruc, "Employing of Hydrophobic Membrane for Collecting of Gases in the Planar Electrolyzer," presented at the 2nd International Congress of Academic Research, Bolu, February 2020.